



저작자표시 2.0 대한민국

이용자는 아래의 조건을 따르는 경우에 한하여 자유롭게

- 이 저작물을 복제, 배포, 전송, 전시, 공연 및 방송할 수 있습니다.
- 이차적 저작물을 작성할 수 있습니다.
- 이 저작물을 영리 목적으로 이용할 수 있습니다.

다음과 같은 조건을 따라야 합니다:



저작자표시. 귀하는 원저작자를 표시하여야 합니다.

- 귀하는, 이 저작물의 재이용이나 배포의 경우, 이 저작물에 적용된 이용허락조건을 명확하게 나타내어야 합니다.
- 저작권자로부터 별도의 허가를 받으면 이러한 조건들은 적용되지 않습니다.

저작권법에 따른 이용자의 권리는 위의 내용에 의하여 영향을 받지 않습니다.

이것은 [이용허락규약\(Legal Code\)](#)을 이해하기 쉽게 요약한 것입니다.

[Disclaimer](#) 

**Amelioration of Alzheimer's disease-like
pathology and cognitive impairment
by regulating systemic metabolism**

A Young Sim

**The Graduate School
Yonsei University
Department of Medical Science**

**Amelioration of Alzheimer's disease-like
pathology and cognitive impairment
by regulating systemic metabolism**

**A Dissertation Submitted
to the Department of Medical Science
and the Graduate School of Yonsei University
in partial fulfillment of the
requirements for the degree of
Doctor of Philosophy in Medical Science**

A Young Sim

June 2024

**This certifies that the Dissertation
of A Young Sim is approved.**



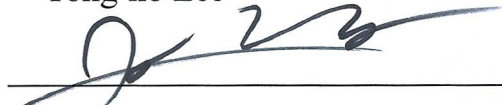
Thesis Supervisor Jong Eun Lee



Thesis Committee Member Chul Hoon Kim



Thesis Committee Member Yong-ho Lee



Thesis Committee Member Hosung Jung



Thesis Committee Member Ho-Taek Song

**The Graduate School
Yonsei University
June 2024**

ACKNOWLEDGEMENTS

I am filled with emotions as I write this letter of gratitude looking back my five-year degree courses.

I started with a heart full of passion and curiosity for science, but as I watched the number of people leaving the laboratory one by one, I was caught up in anxiety and complacency, wondering if I would be left alone. Every time I felt like giving up, I tried to pull myself together by remembering the time I first set foot in the laboratory. It is very meaningful that the results have come to fruition as a doctoral dissertation.

I would like to take this opportunity to express my gratitude to those who have supported me along the way.

First and foremost, I would like to express my deepest gratitude to my advisor, Professor Jong Eun Lee. The summer of 2017, when I first met Professor Jong Eun Lee, remains vivid in my memory as if it were just yesterday. I was immediately drawn to Professor Jong Eun Lee's remarkable presence as a scientist, and I knew without hesitation that I wanted to become Professor's student. I would like to take this opportunity to convey that sentiment. I am grateful for instilling in me the true essence of science and the qualities of an authentic researcher, from the beginning of my academic journey, including my internship, up to this moment.

Furthermore, I would give my sincere appreciation to Professor Yong-ho Lee for consistently offering valuable advice amidst his busy schedule, which has contributed significantly to the improvement of my research and the refinement of this thesis. And I am deeply grateful to Professor Chul Hoon Kim, Professor

Hosung Jung, and Professor Ho-Taek Song for their guidance and for filling the gaps in my paper through their insightful evaluation as members of my thesis committee.

Secondly, I also extend my gratitude to the lab family, including my colleagues and seniors, who have walked alongside me throughout my academic journey.

Especially, I would like to extend thank Dr. Jong Youl and Jiwon, who have been more than just lab members but mentors in life, spending even more time with me over the past five years than my own family. I will miss the countless lunch hours and gatherings we shared together. I also would also like to thank Dr. Sumit, who taught me many things since I first entered the lab.

I will cherish all the connections I made during my time in the lab and hold them close to my heart.

Additionally, I want to give my special thanks to my better half, who promised a new beginning on the last page of a chapter, for enabling me to finish the final pages smoothly.

Last but not least, I would like to express this sentiment to our dear family, who have always believed in and supported me.

I would like to thank my grandmother, who has always proudly regarded me as her granddaughter. I also want to express my gratitude to my younger sister, Ha Young, who has been more mature than me.

My pillars of strength, my parents, who have unconditionally supported and loved me, patiently waiting and encouraging me through it all. Through this letter, I would like to take this opportunity to express my deepest deep appreciation and heartfelt

apologies for being able to successfully complete my degree program because of you.

Though this brief message cannot fully express my gratitude, I extend my deepest thanks once again to everyone who has contributed to my dissertation.

No matter where I am, I will never forget my original intention to become a true scientist with a pure heart and a humble attitude of always wanting to learn when I first encountered science.

Additionally, I will continue to reflect on all the lessons learned during this journey and strive to grow into a better person.

June 2024

A Young Sim

TABLE OF CONTENTS

LIST OF FIGURES	iv
LIST OF TABLES	vi
ABSTRACT	vii
1. INTRODUCTION	1
2. MATERIALS AND METHODS	6
2.1. Animals	6
2.2. Drug treatment	6
2.3. Measurement of blood glucose level (BG) and body weight (BW)	8
2.4. Insulin tolerance test (ITT) and glucose tolerance test (GTT)	8
2.5. Measurement of serum insulin levels and insulin resistance	8
2.6. Behavioral test	9
2.6.1. Novel object recognition test (NORT)	9
2.6.2. Morris water maze (MWM)	9
2.7. ¹⁸ F-fluorodeoxyglucose (¹⁸ F-FDG)-positron-emission tomography (PET)	10
2.8. Brain sample preparation	10
2.9. Western blotting (WB)	10
2.10. Immunohistochemistry (IHC)	11
2.11. Antibodies	12
2.12. Proteome profiler mouse cytokine array	12

2.13. Quantitative polymerase chain reaction (qPCR)	13
2.14. Statistical analysis	13
3. RESULTS	16
<i>Part 1. Restoration of brain insulin signaling by SGLT2-i and DPP4-i improved</i>	
cognitive and memory functions	16
3.1. SGLT2-i and DPP4-i exerted metabolic benefits in T2D-AD mouse model	16
3.2. SGLT2-i and DPP4-i restored brain insulin signaling via IRS1/Akt/GSK3 β	
pathway	21
3.3. SGLT2-i and DPP4-i changed glucose utilization in the brain	26
3.4. SGLT2-i and DPP4-i increased ketone metabolic in the brain	29
3.5. SGLT2-i and DPP4-i improved hippocampal-dependent cognitive functions	31
3.6. SGLT2-i and DPP4-i reduced pTau and A β accumulation in the brain	36
3.7. SGLT2-i reduced pTau level by activating ACE2/Ang (1-7)/MasR, whereas	
DPP4-i decreased A β accumulation by increasing IDE level	40
<i>Part 2. Brain metabolic changes caused by SGLT2-i and DPP4-i influenced brain</i>	
inflammatory responses	44
3.8. SGLT2-i and DPP4-i reduced pro-inflammatory cytokines in the brain	44
3.9. SGLT2-i and DPP4-i induced microglia to M2 phenotype	49
3.10. SGLT2-i and DPP4-i altered the phenotype of microglia by inhibiting NLRP3	
inflammasome	51
3.11. SGLT2-i suppressed NLRP3 inflammasome by regulating the binding of pTau	

and CX3CR1, whereas DPP4-i suppressed NLRP3 inflammasome by regulating the binding of A β and TLR4	53
4. DISCUSSION	56
5. CONCLUSION	64
REFERENCES	65
APPENDICES	74
ABSTRACT IN KOREAN	76

LIST OF FIGURES

<Figure 1> Establishment of T2D-AD mouse model and experimental timeline	7
<Figure 2> A 60% HFD and STZ induced T2D-AD mouse model in C57BL/6	18
<Figure 3> SGLT2-i and DPP4-i reduced BG and BW	19
<Figure 4> SGLT2-i and DPP4-i improved peripheral insulin resistance	20
<Figure 5> SGLT2-i and DPP4-i improved brain insulin signaling pathway: IRS1	23
<Figure 6> SGLT2-i and DPP4-i improved brain insulin signaling pathway: Akt	24
<Figure 7> SGLT2-i and DPP4-i improved brain insulin signaling pathway: GSK3 β	25
<Figure 8> SGLT2-i and DPP4-i altered brain glucose uptake	27
<Figure 9> SGLT2-i and DPP4-i increased GLUTs	28
<Figure 10> SGLT2-i and DPP4-i affected brain ketone metabolism	30
<Figure 11> SGLT2-i and DPP4-i improved learning and memory functions: NORT	33
<Figure 12> SGLT2-i and DPP4-i improved learning and memory functions: MWM	34
<Figure 13> SGLT2-i and DPP4-i regulated tau phosphorylation	38
<Figure 14> SGLT2-i and DPP4-i reduced A β accumulation	39
<Figure 15> SGLT2-i reduced tau phosphorylation by activating ACE2/Ang (1-7)/MasR	42
<Figure 16> DPP4-i reduced A β accumulation by increasing IDE level	43
<Figure 17> SGLT2-i and DPP4-i altered microglial activity	46
<Figure 18> SGLT2-i and DPP4-i reduced anti-inflammatory cytokines	47

<Figure 19> SGLT2-i and DPP4-i suppressed M1-induced cytokines and increased M2-induced cytokines	48
<Figure 20> SGLT2-i and DPP4-i changed the phenotype of microglia	50
<Figure 21> SGLT2-i and DPP4-i suppressed NLRP3 inflammasome activation	52
<Figure 22> SGLT2-i suppressed NLRP3 inflammasome by regulating pTau and CX3CR1 binding	54
<Figure 23> DPP4-i suppressed NLRP3 inflammasome by regulating A β and TLR4 binding	55

LIST OF TABLES

<Table 1> The qPCR analysis primers of ketone bodies	15
--	----

ABSTRACT

Amelioration of Alzheimer's disease-like pathology and cognitive impairment by regulating systemic metabolism

Alzheimer's disease (AD) and type 2 diabetes mellitus (T2D) share a number of common features, including insulin resistance and inflammatory responses. Insulin resistance in the brain is known to be a key factor in the pathogenesis of AD. Recent studies have demonstrated that anti-diabetic drugs, specifically sodium–glucose cotransporter-2 inhibitor (SGLT2-i) and dipeptidyl peptidase-4 inhibitor (DPP4-i) improve insulin sensitivity and provide neuroprotection. However, the exact mechanism through which these two inhibitors affect the brain metabolism remain uninvestigated.

In this study, the T2D-AD mouse model using a 60% high-fat diet (HFD) for 19 weeks along with a single dose of streptozotocin (100 mg/kg, intraperitoneally) at the fourth week of a 60% HFD initiation were treated with SGLT2-i (empagliflozin; 25 mg/kg/day, orally [PO]) and DPP4-i (sitagliptin; 100 mg/kg/day, PO) for 7 weeks. SGLT2-i and DPP4-i reduced blood glucose level and body weight, effectively ameliorated insulin sensitivity, and significantly improved hippocampal-dependent learning, memory, and cognitive functions in the T2D-AD mouse model. Interestingly, SGLT2-i and DPP4-i significantly affected the reduction of hyperphosphorylated tau (pTau) protein and amyloid β (A β) accumulation, respectively. SGLT2-i reduced pTau accumulation through the angiotensin converting enzyme-2/angiotensin (1-7)/mitochondrial assembly receptor axis, whereas DPP4-i reduced A β accumulation by increasing insulin-degrading enzyme levels. In addition, changes in glucose and ketone metabolism induced by SGLT2-i and DPP4-i inhibited NLR family pyrin domain containing 3 (NLRP3) inflammasome regulation in microglia, thereby altering microglial activation. SGLT2-i and DPP4-i influenced NLRP3 inflammasome in microglia via C-

X3-C motif chemokine receptor 1 and toll-like receptor 4, respectively, converting their phenotype and ameliorating neuroinflammatory responses induced by pTau and A β accumulation.

These findings suggest that SGLT2-i and DPP4-i regulate neurodegeneration by participating brain insulin signaling and inflammatory responses and have implications for preventing AD-like pathology and cognitive dysfunction in T2D-AD mice via distinct mechanisms.

Key words : Alzheimer's disease, type 2 diabetes disease, sodium–glucose cotransporter-2 inhibitor, dipeptidyl peptidase-4 inhibitor, insulin signaling, neuroinflammation

1. INTRODUCTION

Dementia is a term that encompasses a variety of symptoms, and there are multiple causes of dementia. Alzheimer's disease (AD) is the most common cause of dementia, accounting for 60-80% of cases.¹ AD is a progressive, irreversible neurological disorder characterized by memory loss, slowed thinking and reasoning, and changes in mood, personality, and behavior.² Furthermore, AD is neuropathologically characterized by the accumulation of abnormal amyloid β ($A\beta$) protein outside neurons and neurofibrillary tangles composed of hyperphosphorylated tau (pTau) protein inside neurons. These changes lead to neuronal damage and destruction, known as neurodegeneration.³

$A\beta$ is a protein fragment derived from amyloid precursor protein (APP) through enzymatic processing. In healthy neurons, APP is digested by α - and γ -secretases, generating some soluble polypeptides that can be broken down and recycled within the cell.⁴ In healthy individuals, there is no imbalance in the production and clearance of $A\beta$. However, in AD, there is an imbalance between the production and clearance of $A\beta$. When β -secretase and γ -secretase complex together to cleave APP, they generate insoluble $A\beta$, which aggregates and leads to the accumulation of $A\beta$ plaques.⁵ The accumulation of $A\beta$ can disrupt neuronal communication at synapses and damage neurons.

Tau is a protein essential for stabilizing microtubules, which maintain the structure of the cell and facilitate intracellular transport within neurons.⁶ Tau can be phosphorylated by tau kinases, particularly glycogen synthase kinase-3 β (GSK3 β).⁷ In AD, tau protein becomes abnormally hyperphosphorylated, leading to the formation of insoluble tangles or aggregates within cells. Tau tangles within neurons obstruct the transport of nutrients and other molecules, which are crucial for the normal function and survival of neurons.

AD can be divided into two clinical subtypes. Both types exhibit similar pathological phenotypes, such as the presence of $A\beta$ plaques and neurofibrillary tangles (NFTs), synaptic damage, and neuronal loss, but the factors triggering the neurodegenerative process differ significantly.⁸

The first subtype is familial AD (fAD), which is caused by autosomal dominant mutations. There are three genes responsible for these autosomal dominant mutations: the APP gene on chromosome 21, the presenilin-1 (PSEN1) gene on chromosome 14, and the PSEN2 gene on chromosome 1. fAD accounts for only 1-2% of all AD cases.

The second subtype, which appears to have weak or no genetic cause, generally occurs sporadically in individuals over 65 years of age and is defined as sporadic AD (sAD). Affecting over 95% of AD patients, sAD is associated with oxidative stress-induced cellular damage, mitochondrial structural and functional abnormalities, inflammatory responses, and aging. While A β and pTau are pathological hallmarks of sAD, it remains unclear whether these factors cause AD or are consequences of the disease. Therefore, various perspectives have emerged to explain sAD.

One of the most common metabolic disorders, type 2 diabetes mellitus (T2D), like sAD, is experiencing an increasing prevalence worldwide. T2D is influenced by various factors but fundamentally involves inappropriate insulin secretion by pancreatic β cells and insulin resistance.⁹

Insulin is the most crucial biological hormone that globally regulates energy metabolism, including carbohydrates, lipids, and proteins, and is also involved in growth and electrolyte regulation. Insulin resistance can be defined as a metabolic state in which insulin sensitivity is reduced at physiological insulin concentrations.¹⁰ Insulin is secreted by pancreatic β cells postprandially to promote glucose uptake in muscles, inhibit glucose production in the liver to regulate blood glucose level, and suppress lipolysis in adipose tissue to store ingested energy. Insulin resistance refers to a state where these insulin actions are diminished despite adequate insulin levels.¹¹

Insulin resistance related to T2D is considered a risk factor for AD. Insulin binds to receptors present in most cells, inducing cellular activity. The insulin receptor is a transmembrane glycoprotein receptor consisting of two extracellular α and two β subunits. When insulin binds to the α subunit of the receptor, multiple tyrosine residues in the cytoplasmic region of the β subunit undergo activation and autophosphorylation. These autophosphorylated residues are recognized by insulin receptor substrates (IRS), with IRS1 and IRS2 acting as primary

mediators of insulin signaling. IRS1 and IRS2 recruit and activate the phosphoinositide 3-kinases (PI3K) complex, which phosphorylates and activates key nodes in the insulin signaling pathway, such as protein kinase B (Akt) and protein kinase C ζ (PKC ζ) and PKC λ . Activated Akt has many downstream effects. It is involved in systemic glucose regulation and regulates various aspects of protein and lipid synthesis, cellular metabolism, growth, survival, and autophagy through mammalian target of rapamycin (mTOR). It phosphorylates GSK3 β , inhibiting the constitutive activity of this key kinase, which plays an important role in cell proliferation, migration, glucose regulation, apoptosis, and neuroplasticity. Additionally, Akt activation directly activates proteins like the inhibitor of nuclear factor- κ B kinase (IKK).^{12,13}

The complexity of insulin action plays a significant role in the brain due to the specialized functions of various brain regions, cell types, and network connections. Under normal conditions, insulin signaling pathways inhibit the production of A β and the pTau protein by inhibiting GSK3 β phosphorylation. However, insulin resistance and deficiency abnormally modulate insulin signal transduction regarding the dysfunction regulation of the PI3K/Akt/GSK3 β signaling pathway. Increased GSK3 β activation can lead to pTau, a critical component of neurofibrillary tangles.¹

Additionally, T2D induces metabolic issues in the brain and other target tissues through a series of pathogenic processes such as oxidative stress, inflammatory responses, and autophagy dysfunction. It is also associated with excessive immune system activation, which increases the expression of inflammatory cytokines in the brain, particularly by microglia. In the AD brain, microglia and astrocytes are known to accumulate around neurofibrillary tangles and are associated with tissue damage occurring in AD. A β oligomers and fibrils can bind to receptors expressed by microglia, including cluster of differentiation 14 (CD14), CD36, CD47, α 6 β 1 integrin, and toll-like receptor (TLR). When A β binds to CD36 or TLR4, it triggers the production of inflammatory chemokines and cytokines, leading to increased neuronal damage in vulnerable regions of the AD brain. Furthermore, pTau is closely associated with pro-inflammatory cytokines.¹⁴⁻¹⁶

Considering the evidence linking AD and T2D, it has been suggested that controlling blood glucose level might potentially prevent AD. Consequently, medications used to treat T2D have

been identified as potential candidates for AD treatment. Most T2D patients require insulin therapy or medication to control their target blood glucose level. These medications include metformin, sulfonylureas, thiazolidinediones, sodium-glucose cotransporter-2 inhibitor (SGLT2-i) and dipeptidyl peptidase-4 inhibitor (DPP4-i).¹⁷

Anti-diabetic drugs are generally classified into two groups based on their primary mechanisms of action: hypoglycemic agents and antihyperglycemic agents. Hypoglycemic agents such as insulin and sulfonylureas act by directly lowering blood glucose level through stimulation of insulin secretion from pancreatic beta cells. In contrast, antihyperglycemic agents, which include metformin, thiazolidinediones, SGLT2-i, DPP4-i and glucagon-like peptide-1 (GLP-1) receptor (GLP-1R) agonists, act by decreasing blood glucose level. The diverse mechanisms of action of antihyperglycemic agents suggest that some of these drugs may have additional therapeutic benefits, such as neuroprotective effects, beyond their glucose-lowering effects.¹⁸

SGLT2-i decreases blood glucose level by increasing glucose and sodium excretion in the urine, which leads to weight loss and reduced blood pressure, thus improving insulin resistance and preserving β cell function by reducing glucose toxicity. Incretins such as glucose-dependent insulinotropic polypeptide (GIP) and GLP-1 are rapidly degraded into inactive forms by the enzyme DPP4 after being secreted from the gut. DPP4 is secreted by the vascular endothelial cells of the intestinal submucosa and the hepatic veins, breaking down incretins, with only 20% of the secreted incretins entering systemic circulation. DPP4-i is hypoglycemic agents that regulate blood glucose level by inhibiting DPP4 enzyme activity, thereby increasing the activity of GLP-1 and GIP, and subsequently enhancing insulin secretion.^{10,19,20}

Recent studies have shown that SGLT2-i and DPP4-i may have additional neuroprotective effects beyond their glucose-lowering properties. These inhibitors were effective in suppressing inflammation and showed benefits in preventing cardiovascular diseases and renal failure. They have also been reported to be effective in reducing neuroinflammation, improving synaptic plasticity, and promoting neuronal survival. However, their therapeutic roles and mechanisms in AD are not yet fully understood.^{21,22}

Therefore, this study aims to understand the pathological mechanisms linking AD and T2D, specifically investigating how insulin resistance, metabolic issues, and inflammatory responses

resulting from T2D influence the onset and progression of AD. Furthermore, the study aims to explore the potential effects of currently used T2D medications on the prevention and treatment of AD. In particular, it aims to explore how anti-diabetic drugs can suppress neuroinflammation and promote neuronal survival, and how these mechanisms can be applied to AD.

2. MATERIALS AND METHODS

2.1. Animals

Male C57BL/6 mice (8 weeks old) were purchased from Central Lab Animal Inc. (Seocho, Seoul, Republic of Korea) and housed under a 12-hour light/dark cycle with humidity- and temperature-controlled environment. Water was provided *ad libitum* throughout the experiment. After a week of acclimatization, the mice were randomly divided into two groups and fed two different diets for 19 weeks: a normal chow diet (ND, 13.1% kcal fat) and a high-fat diet (HFD, 60% kcal fat, Research Diet, New Brunswick, NJ, USA). The mice fed a 60% HFD were injected once with a low dose of streptozotocin (STZ, 100 mg/kg, intraperitoneally [IP], Sigma-Aldrich, St. Louis, MO, USA) dissolved in citrate buffer (pH 4.4, Sigma-Aldrich) at week 4 to establish T2D by inducing partial insulin deficiency. All animal experiments were performed in accordance with the guidelines and approved by the Institutional Animal Care and Yonsei Laboratory Animal Research Center (IACUC approval no. 20220045).

2.2. Drug treatment

At week 12, mice with fasting blood glucose level > 250-300 mg/dL, body weight > 45 g, and impaired insulin and glucose tolerance were classified as T2D mice. These mice were randomly assigned to one of the following three groups: vehicle (0.5% carboxymethylcellulose, Sigma-Aldrich), SGLT2-i (empagliflozin; 25 mg/kg/day, orally [PO]), or DPP4-i (sitagliptin; 100 mg/kg/day, PO). The drugs were administered to the mice for 7 weeks, and the mice in the ND group were administered the vehicle for the same period (Fig. 1).

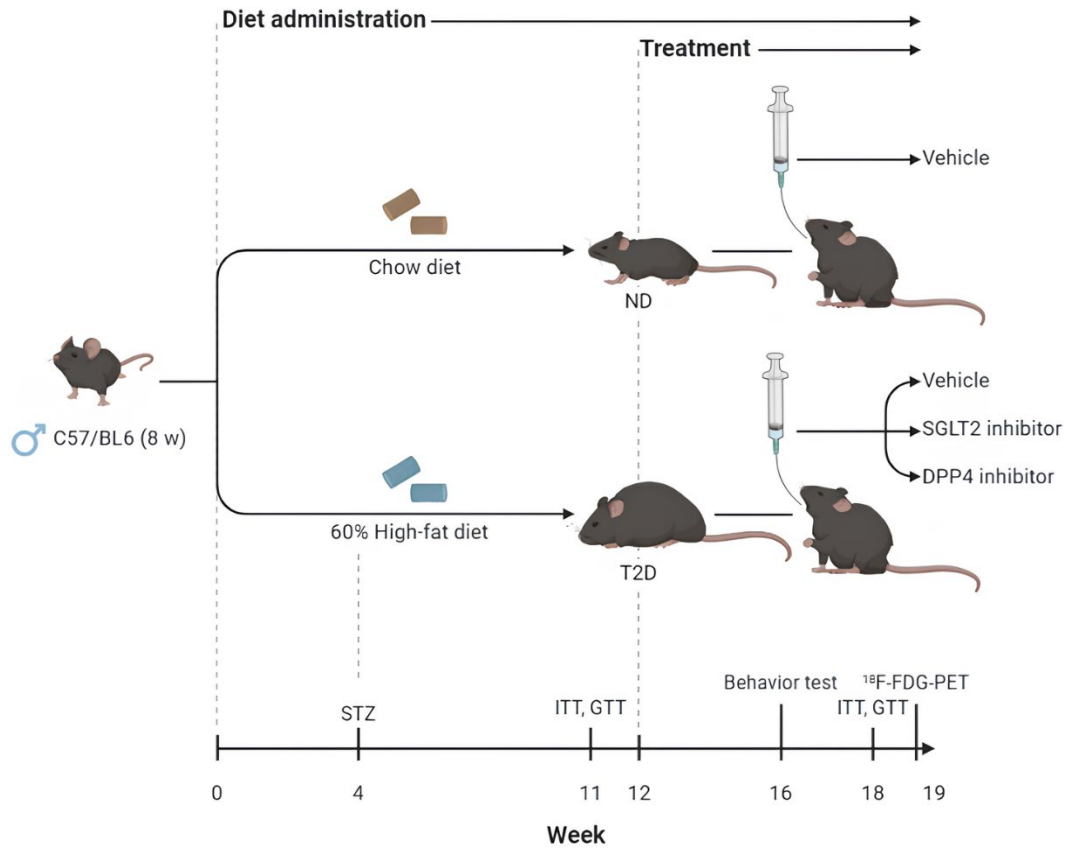


Figure 1. Establishment of T2D-AD mouse model and experimental timeline. The mice were randomly divided into two groups and fed two different diets for 19 weeks: a ND and a 60% HFD with STZ. At week 12, the T2D mice were randomly assigned to one of the following three groups: vehicle, SGLT2-i or DPP4-i and were administered the drugs for 7 weeks. Each experiment was conducted over time in all groups.

2.3. Measurement of blood glucose level (BG) and body weight (BW)

The BG and BW of the mice were recorded at the same time every week. Prior to recording, the mice were transferred to empty cages and fasted for 4 hours. Blood samples were collected by cutting off the tip of the tail, and the BG was measured using a glucometer (Accu-Chek, Roche Diagnostics Corp., Indianapolis, IN, USA).

2.4. Insulin tolerance test (ITT) and glucose tolerance test (GTT)

The ITT and GTT were conducted once in weeks 12 and 18. For the ITT, the mice were transferred to empty cages around 9 a.m. and fasted for 4 hours before the test. Insulin (0.75 U/kg, Sigma-Aldrich) dissolved in saline (Dai Han Pham Co., Yeongdeungpo, Seoul, Republic of Korea) was injected IP. Blood samples were collected from the tail tip, and the BG was measured using a glucometer (Accu-Chek) at 0, 15, 30, 60, 90, and 120 minutes post-injection. The GTT was performed two days after the ITT. The mice were transferred to empty cages around 9 a.m. and fasted for 6 hours before the test. Glucose (2 g/kg, Sigma-Aldrich) dissolved in saline (Dai Han Pham Co.) was injected IP. Blood samples were collected from the tail tip, and the BG was measured using a glucometer (Accu-Chek) at 0, 15, 30, 60, 90, and 120 minutes post-injection.

2.5. Measurement of serum insulin levels and insulin resistance

Fasting serum insulin levels were measured using a mouse insulin enzyme-linked immunosorbent assay kit (Morinaga Institute of Biological Science, Yokohama, Kanagawa, Japan), according to the manufacturer's instructions. Insulin sensitivity was assessed using a homeostatic model assessment for insulin resistance (HOMA-IR) index, calculated as follows: $HOMA-IR = (\text{fasting serum insulin } [\mu\text{U/mL}] \times \text{fasting serum glucose } [\text{mmol/L}]) / 22.5$.

2.6. Behavioral tests

2.6.1. Novel object recognition test (NORT)

The NORT is a widely used behavioral test for evaluating learning and memory functions in mice. The NORT was conducted in a square arena ($40 \times 40 \times 40$ cm) over a period of three days encompassing habituation, training, and probe test phases. Before the test, the mice had an acclimatization period of 30 minutes. During the habituation, the mice were removed from their home cages and placed in an empty arena for 5 minutes. During the training session, identical objects were placed in opposite quadrants of the arena and the mice were allowed to explore two identical objects for 5 minutes. On the test day, one of the objects used during the training was replaced with a novel object and the mice were allowed to explore the two objects freely for 10 minutes. The arena and the objects were washed with 70% ethanol after each trial to minimize olfactory cues. Animal behavior was analyzed using a video tracking software, SMART 3.0 (PanLab, Holliston, MA, USA).

2.6.2. Morris water maze (MWM)

The MWM was performed to evaluate hippocampal-dependent learning, including the acquisition of spatial memory. The MWM was carried out over six days in a circular tank (100 cm in diameter and 35 cm in depth) filled with water ($22\text{--}25^\circ\text{C}$) mixed with white paint, in a soundproof and dimly lit room. Before the test, the mice underwent a 30-minute acclimatization period. On the first day, the mice were placed in a pool and habituated to the water for 60 seconds. During the training period, a platform was placed inside the pool and four positions were designated on the pool wall: north (N), south (S), east (E), and west (W). The mice were trained four times a day for four consecutive days. Each day, the mice started by facing N, S, E, and W sequentially. A trial concluded when the mice located the platform or after 60 seconds had elapsed. The mice that found the platform within 60 seconds were moved to the cage, while those that did not find the platform were placed on it after 60 seconds and then moved to the cage. On the sixth day, the mice were allowed to swim freely for 90 seconds in the pool without the platform to locate the area where the platform had been. Animal behavior was analyzed using a video tracking software, SMART 3.0 (PanLab).

2.7. ^{18}F -fluorodeoxyglucose (^{18}F -FDG)-positron-emission tomography (PET)

The mice were fasted overnight prior to the ^{18}F -FDG-PET. Warming was achieved by placing the mice on a heating pad maintained at 30°C for at least 30 minutes before ^{18}F -FDG injection. After anesthetizing the mice with 2% inhaled isoflurane gas, an intravenous catheter was inserted into the tail vein, and 200-250 μCi of ^{18}F -FDG was injected through it. Then, the mice were allowed to rest on a heating pad for 45 minutes. The ^{18}F -FDG-PET data were acquired using the Inveon Dedicated PET (Siemens Aktiengesellschaft, Munich, Bayern, German) for a duration of 10 minutes. After imaging, the mice were kept under a heat lamp until fully awake and then placed in an isolation room for 24 hours to eliminate radiation hazards. Image analysis was conducted using an AMIDE software (Sourceforge, San Diego, CA, USA).

2.8. Brain sample preparation

The mice were randomly assigned to either the western blotting (WB) or immunohistochemistry (IHC) groups. The mice were deeply anesthetized with an IP. injection of a mixture of zoletil (100 mg/kg, Virbac, Carros, Alpes-Maritimes, France) and xylazine (Rompun; 10 mg/kg, Elanco, Greenfield, IN, USA). For the WB, the mice were transcardially perfused with saline (Dai Han Pham Co.). The whole brain was dissected, and the cortex (CTX) and hippocampus (HIP) were isolated and frozen in liquid nitrogen, followed by storage at -80°C until further experiments. For the IHC, the mice were transcardially perfused with saline (Dai Han Pham Co.) and 4% paraformaldehyde (PFA, Sigma-Aldrich) in 1X phosphate-buffered saline (PBS, Biosesang, Yongin-si, Gyeonggi-do, Republic of Korea). The brains were extracted and incubated in 4% PFA (Sigma-Aldrich) for 24 hours at 4°C. The fixed brain tissues were placed in 30% sucrose for 1-3 days at 4°C and stored at -80°C until further experiments.

2.9. Western blotting (WB)

The CTX and HIP tissues were lysed in ice-cold radioimmunoprecipitation assay buffer (Tech & Innovation, chuncheon-si, gangwon-do, Republic of Korea) containing phosphatase

and protease inhibitor cocktail solution (GenDEPOT, Baker, TX, USA) using a homogenizer. Protein concentration was determined using the bicinchoninic acid assay. Each sample containing 50 μ g of protein was separated by 10% sodium dodecyl sulfate-polyacrylamide gel electrophoresis and electroblotted onto a polyvinylidene difluoride membrane (Millipore, Burlington, MA, USA). The membranes were blocked with 5% bovine serum albumin (BSA, GenDEPOT) at room temperature for 1 hour to prevent nonspecific binding, followed by an overnight incubation with the primary antibodies at 4°C. After washing thrice with tris-buffered saline (TBS) containing 0.5% tween 20 (TBS-T, GenDEPOT), the membranes were incubated with the horseradish peroxidase (HPR)-conjugated IgG (H+L) secondary antibodies at room temperature for 2 hours. After washing thrice with 0.5% TBS-T (GenDEPOT), signals were detected using an ECL reagent (GenDEPOT) and visualized using an LAS 4000 mini (Fujifilm Life Science USA, Stamford, CT, USA).

2.10. Immunohistochemistry (IHC)

The brain hemispheres were freshly embedded with Tissue-Tek® O.C.T. compound (Sakura Finetek, Chuo-ku, Tokyo, Japan) within cryomolds and subsequently frozen. The frozen tissues were sectioned into 14- μ m thick slices. The sections were fixed in cold methanol for 15 minutes at -20°C. After washing thrice with 1X PBS (Biosesang), the sections were permeabilized with 1X PBS (Biosesang) containing 0.25% triton X-100 (Sigma-Aldrich) for 30 minutes. After washing thrice with 1X PBS (Biosesang), the sections were blocked with 5% BSA (GenDEPOT) for 1 hour at room temperature to block nonspecific binding. Then, the sections were incubated with the primary antibodies overnight at 4°C. After incubation, the sections were washed with 1X PBS (Biosesang) thrice and incubated with the appropriate secondary antibodies for 2 hours at room temperature in a dark chamber. The sections were washed thrice with 1X PBS (Biosesang), stained with 6-diamidino-2-phenylindole (DAPI, Thermo Fisher Scientific, Waltham, MA, USA) for 5 minutes at room temperature in a dark chamber, and washed again thrice with 1X PBS (Biosesang). Images were acquired using an LSM 710 microscope (Carl Zeiss, Oberkochen, Baden-Württemberg, Germany).

2.11. Antibodies

The Following primary antibodies were used in this study: phospho-IRS1 (pIRS1, Santa Cruz, Santa Cruz, CA, USA), IRS1 (Abcam, Cambridge, Cambridgeshire, England), phospho-Akt (pAkt, Invitrogen, Waltham, MA, USA), Akt (Santa Cruz), phospho-GSK3 β (pGSK3 β , Abcam), GSK3 β (Abcam), glucose transporter 1 (GLUT1, Invitrogen), GLUT3 (Invitrogen), GLUT4 (Invitrogen), pTau (Santa Cruz), Tau (Abcam), A β (Thermo Fisher Scientific), microtubule-associated protein 2 (MAP2, Abcam), angiotensin converting enzyme-2 (ACE2, Abcam), angiotensin (1-7)/mitochondrial assembly receptor (Ang (1-7)/MasR, Thermo Fisher Scientific), insulin-degrading enzyme (IDE, Abcam), transmembrane protein 119 (TMEM119, Abcam), interleukin 4 (IL-4, Santa Cruz), IL-1 β (Santa Cruz), mannose receptor (CD206, Abcam), CD86 (Abcam), NLR family pyrin domain containing 3 (NLRP3, Invitrogen), microtubule-associated protein 1A/1B-light chain 3 (LC3, Abcam), C-X3-C motif chemokine receptor 1 (CX3CR1, Invitrogen), nuclear factor κ -light-chain-enhancer of activated B cells (NF- κ B, Abcam), GLP-1R (Abcam), β -actin (Abcam).

Following secondary antibodies were used in this study: goat anti-rabbit IgG (H+L) secondary antibody, HRP (Invitrogen), goat anti-mouse IgG (H+L) secondary antibody, HRP (Invitrogen), rabbit anti-goat IgG (H+L) secondary antibody, HRP (Invitrogen), donkey anti-rabbit IgG (H+L) cross-adsorbed secondary antibody, rhodamine (Invitrogen), donkey anti-rabbit IgG (H+L) cross-adsorbed secondary antibody, Alexa fluor 555 (Invitrogen), donkey anti-goat IgG (H+L) cross-adsorbed secondary antibody, FITC (Invitrogen), goat anti-mouse IgG (H+L) cross-adsorbed secondary antibody, rhodamine (Invitrogen), goat anti-mouse IgG (H+L) cross-adsorbed secondary antibody, FITC (Invitrogen), goat anti-rat IgG (H+L) cross-adsorbed secondary antibody, rhodamine (Invitrogen), donkey anti-rat IgG (H+L) cross-adsorbed secondary antibody, FITC (Invitrogen).

2.12. Proteome profiler mouse cytokine array

To evaluate the relative expression of cytokines and chemokines in the mice brain, a mouse cytokine array analysis was performed using a mouse cytokine antibody array panel A (R&D Systems, Minneapolis, MN, USA) according to the manufacturer's instructions. Signals were detected using a chemi reagent mix (R&D Systems) and visualized using an LAS 4000 mini

(Fujifilm Life Science USA). Positive signals were quantified with a QuickSpots (Ideal Eyes Systems, Bountiful, UT, USA).

2.13. Quantitative polymerase chain reaction (qPCR)

Total RNA was isolated from frozen tissues using a TRIzol reagent (Ambion, carlsbad, CA, USA). A 40 mg sample of frozen tissue was incubated in 400 μ L of a TRIzol reagent (Ambion) for 5 minutes and then homogenized. After homogenization, 80 μ L of chloroform (Sigma-Aldrich) was added, and the mixture was vortexed at room temperature at 5-minute intervals for a total incubation time of 15 minutes. The sample was centrifuged at 13,000 rpm for 15 minutes at 4°C. The supernatant was transferred to a new tube, followed by the addition of 400 μ L of isopropyl alcohol (Sigma-Aldrich), and incubated at 4°C for 20 minutes. The sample was centrifuged again at 13,000 rpm for 15 minutes at 4°C, and the supernatant was discarded. Then 500 μ L of 70% ethanol was added to the pellet, and the sample was centrifuged at 13,000 rpm for 15 minutes at 4°C. The ethanol was discarded, and the pellet was incubated at room temperature until it was dry. Finally, the RNA pellet was resuspended in 40 μ L of RNase-free water (Invitrogen) and heated at 55°C for 10 minutes. The isolated RNA was reverse transcribed into cDNA using a high-capacity cDNA reverse transcription kit (Applied Biosystems, Waltham, MA, USA), according to the manufacturer's instructions. The qPCR was conducted using a power up SYBR green master mix for qPCR (Applied Biosystems) with the specific primers (Table 1). Relative mRNA expression levels were analyzed using the $\Delta\Delta$ Ct method with a StepOne software version 2.2.2 (Applied Biosystems). 18S rRNA was used as an internal control for normalization.

2.14. Statistical analysis

All statistical analyses were performed using a GraphPad Prism version 8 (Dotmatics, San Diego, CA, USA). A repeated measures one-way analysis of variance analysis (ANOVA) and a one-way ANOVA were used to determine statistical significance and an unpaired t-test was used to compare the means of two groups. All values are expressed as the mean \pm standard error of the mean (S.E.M). $P < 0.05$ was considered statistically significant (#, $P < 0.05$, ##, $P < 0.01$,

###, \$\$\$ $P < 0.001$, ####, \$\$\$\$ $P < 0.0001$, * $P < 0.05$, ** $P < 0.01$, *** $P < 0.001$, and **** $P < 0.0001$).

Table 1. The qPCR analysis primers of ketone bodies

Gene Name	Forward (5' to 3')	Reverse (5' to 3')
<i>HMGCL</i>	ACTACCCAGTCCTGACTCCAA	TAGAGCAGTTCGCGTTCTTCC
<i>HMGCS2</i>	TCAACTCCCTGTGCCTGACA	CAATGATGGTCTCGGTGCCC
<i>MCT1</i>	TGCAACGACCAGTGAAGTATC	GACAACCACCAGCGATCATT
<i>MCT2</i>	ATACTTGCAGGTCCTCTCATTC	GGAAGAGGCAGACAACGATAA
<i>BDH1</i>	TCTCGGACTGCCTGCGCTAT	ACCGCTGTTGCAGTAGGTTT
<i>PPARα</i>	AGAGCCCCATCTGTCTCTC	ACTGGTAGTCTGCAAAACCAAA
<i>SMCT1</i>	AACCAGTCCCAAGTGCAGAGA	ATCACCCAGAGGCCACAA
<i>SMCT2</i>	TGGCATCACAAGCACCTATGA	TACGATGTAGATAATGGTTGCTGC
<i>18S</i>	GATGTGAAGGATGGGAAGTA	CTTCTTGGATACACCCACAG

3. RESULTS

Part 1. Restoration of brain insulin signaling by SGLT2-i and DPP4-i improved cognitive and memory functions

3.1. SGLT2-i and DPP4-i exerted metabolic benefits in T2D-AD mouse model

The T2D-AD mouse model was designed using a 60% HFD and STZ. Various concentrations of STZ were used to induce the T2D mouse model, and prior experiments were conducted with three STZ concentrations: 25 mg for 3 days, 50 mg for 2 days, and a single dose of 100 mg. The preliminary experiments involved dietary intake for 12 weeks, with the STZ administered to the mouse model in the fourth week. There were no significant differences in the BW among the three concentrations at week 12. However, a significant increase in the BG was observed in the group receiving a single dose of 100 mg STZ (Fig. 2A, B). Therefore, for this experiment, a single dose of 100 mg STZ was adopted, and mice with the fasting BG above 250-300 mg/mL were designated as T2D mice.²³

In this experiment, the mice were randomly assigned to either the ND group or HFD groups at week 0. The HFD group received STZ administration at week 4. The T2D mice were selected from the HFD mice at week 12. At week 12, there were visual differences between the ND and T2D groups (Fig. 3A). Compared to the ND group, the T2D groups showed increased the BG and BW until week 12. At week 12, the mice identified as the T2D were randomly assigned to the vehicle, SGLT2-i, and DPP4-i groups for treatment, which continued until week 19. The ND group received vehicle treatment until week 19. From weeks 12 to 19, the BG and BW significantly decreased in the SGLT2-i and DPP4-i groups compared to the vehicle group (Fig. 3B, C). Meanwhile, no changes were observed in the ND group from week 0 to week 19. This indicates that a 60% HFD and STZ induce the T2D-AD mouse model in C57BL/6 mice and that SGLT2-i and DPP4-i provide metabolic benefits.

Furthermore, the ITT and GTT were performed insulin resistance and impaired glucose tolerance in the T2D-AD mouse model, which were improved by SGLT2-i and DPP4-i. At week 11,

compared to the ND group, the T2D groups showed increased the BG in both the ITT and GTT. However, at week 18, the SGLT2-i and DPP4-i groups showed significant decreases in the BG compared to the vehicle group (Fig. 4A, B). Consistent with the ITT results, the HOMA-IR results, reflecting systemic insulin resistance, showed significantly higher values in the vehicle group, which improved in the SGLT2-i and DPP4-i groups (Fig. 4C). In addition, while hyperinsulinemia was observed in the vehicle group, insulin levels decreased in the SGLT2-i and DPP4-i groups (Fig. 4D). Weekly measurements of food intake in each group showed similar consumption levels (Fig. 4E). This indicates that SGLT2-i and DPP4-i treatments do not affect food intake while reducing the BG and BW, improving insulin resistance, and impaired glucose tolerance.

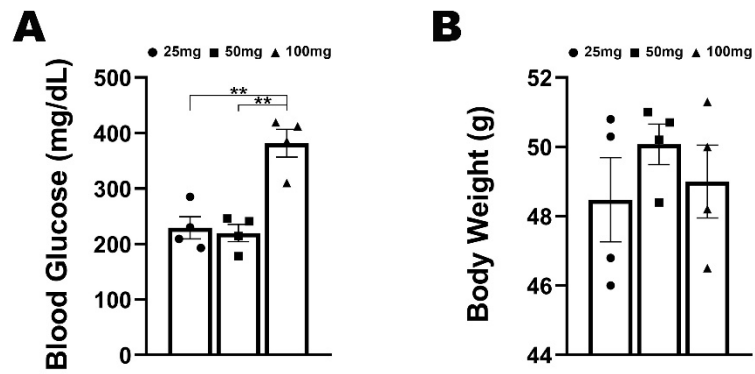


Figure 2. A 60% HFD and STZ induced T2D-AD mouse model in C57BL/6. Comparison of the (A) BG (n = 4) and (C) BW (n = 4) after injection of three doses of STZ. Data are presented as mean \pm S.E.M. $**P < 0.01$.

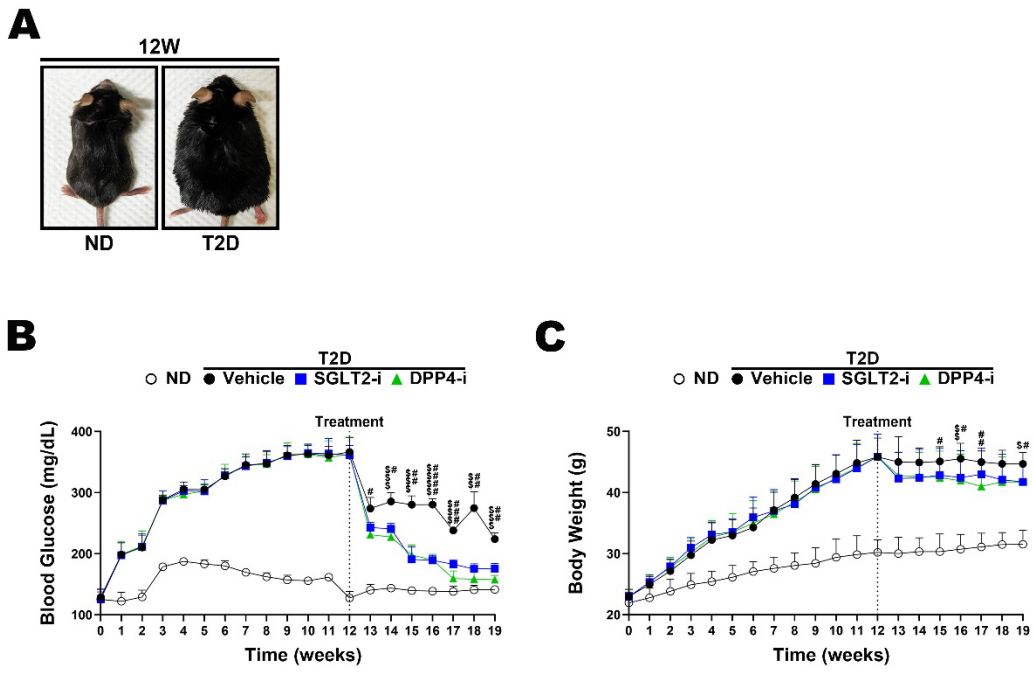


Figure 3. SGLT2-i and DPP4-i reduced BG and BW. (A) Comparison of the ND and T2D groups of mice at week 12. Changes in the (B) BG (n = 8) and (C) BW (n = 8) of all groups over 19 weeks. A repeated measures one-way ANOVA showed a significant increase in the BG and BW in all T2D groups from weeks 1 to 12: $P < 0.0001$. Data are presented as mean \pm S.E.M. #,\$ $P < 0.05$, ##,\$\$ $P < 0.01$, ###,\$\$\$ $P < 0.001$, ####,\$\$\$\$ $P < 0.0001$ compared with the vehicle and the SGLT2-i or DPP4-i groups.

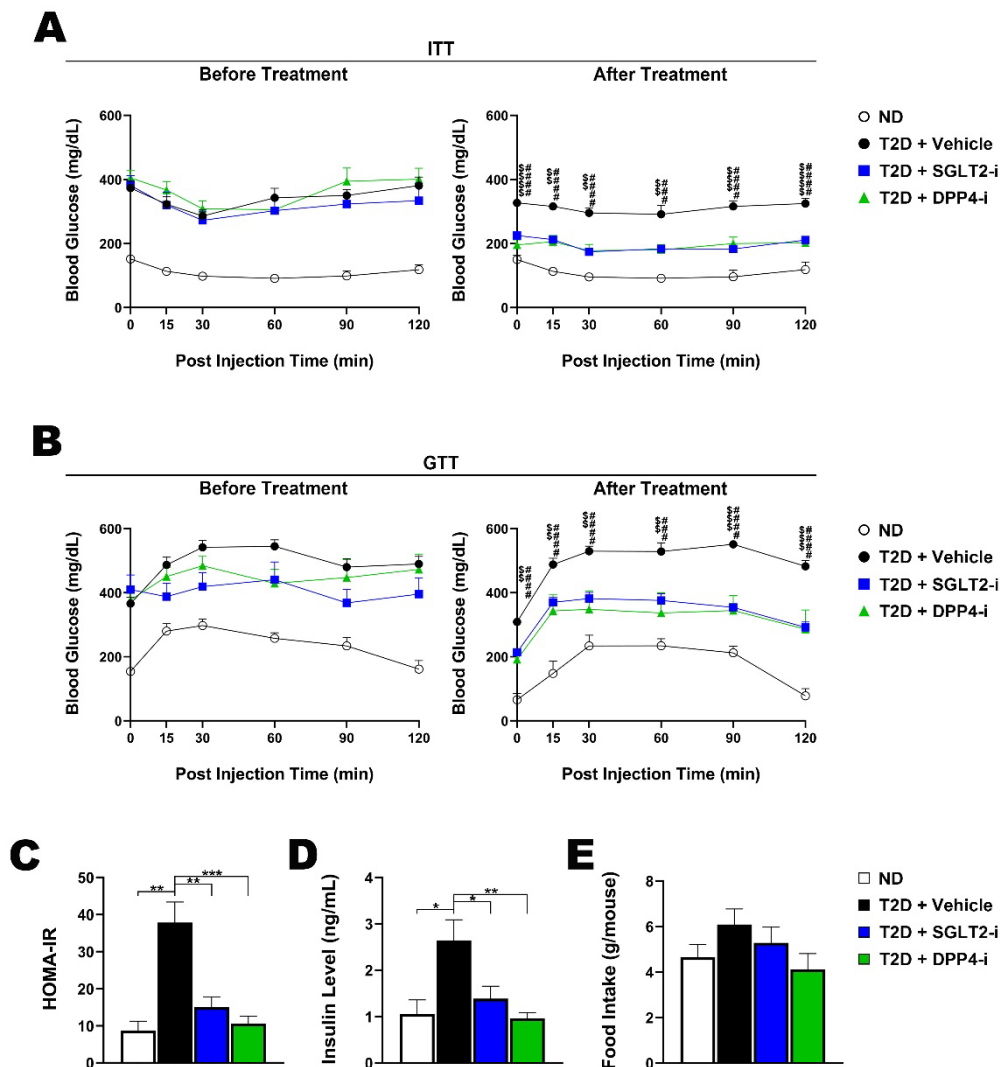


Figure 4. SGLT2-i and DPP4-i improved peripheral insulin resistance. (A) ITT ($n = 8$) and (B) GTT ($n = 8$) performed at weeks 12 and 18. A repeated measures one-way ANOVA showed a significant increase in the BG in all T2D groups: $P < 0.0001$. Data are presented as mean \pm S.E.M. ##,\$\$\$ $P < 0.01$, ###,\$\$\$ $P < 0.001$, ####,\$\$\$ $P < 0.0001$ compared with the vehicle and the SGLT2-i or DPP4-i groups. (C) HOMA-IR ($n = 3$) which represents the insulin resistance index. (D) Serum insulin levels ($n = 3$). (E) Average food intake during 19 weeks ($n = 8$). Data are presented as mean \pm S.E.M. * $P < 0.05$, ** $P < 0.01$, *** $P < 0.001$.

3.2. SGLT2-i and DPP4-i restored brain insulin signaling via IRS1/Akt/GSK3 β pathway

The insulin signaling pathway regulates downstream signaling of IRS1/Akt/GSK3 β .¹⁸ This part aimed to determine whether the peripheral insulin signaling improvements induced by SGLT2-i and DPP4-i also affect the brain insulin signaling. The mice brains were dissected into the CTX and HIPP, and IRS1/Akt/GSK3 β were analyzed using the IHC and WB. For pIRS1, the phosphorylation site pIRS1 (Tyr 632), which is associated with insulin resistance, was examined. In the case of pAkt and pGSK3 β , the phosphorylation sites pAkt (Ser 473) and pGSK3 β (Ser 9), which are related to insulin sensitivity, were investigated.

For the IHC, pIRS1 (Tyr 632) was stained with FITC and IRS1 was stained with rhodamine. The signal intensity of pIRS1 (Tyr 632) was significantly higher in the vehicle group compared to the ND, SGLT2-i, and DPP4-i groups (Fig. 5A). The expression level of pIRS1 (Tyr 632) with a size of 170 kDa was elevated in both the CTX and HIPP of the vehicle group (Fig. 5B). The pIRS1 (Tyr 632)/total IRS1 ratio was increased in both the CTX and HIPP of the vehicle group compared to the ND group. In the SGLT2-i group, this ratio significantly decreased in both the CTX and HIPP, while in the DPP4-i group, it significantly decreased in the HIPP compared to the vehicle group (Fig. 5C).

In the IHC analysis, pAkt (Ser 473) stained with FITC and Akt stained with rhodamine showed unclear pAkt (Ser 473) signal intensity in the CTX and HIPP of the vehicle group (Fig. 6A). The expression level of pAkt (Ser 473) with a size of 60 kDa was increased in the ND, SGLT2-i, and DPP4-i groups compared to the vehicle group in both the CTX and HIPP (Fig. 6B). The pAkt (Ser 473)/total Akt ratio was significantly higher in the ND, SGLT2-i, and DPP4-i groups than in the vehicle group for both the CTX and HIPP (Fig. 6C).

Additionally, in the IHC results for pGSK3 β (Ser 9) stained with FITC and GSK3 β stained with rhodamine, the vehicle group exhibited indistinct pGSK3 β (Ser 9) signal intensity in the CTX and HIPP (Fig. 7A). The expression level of pGSK3 β (Ser 9) with a size of 46 kDa was increased in the ND, SGLT2-i, and DPP4-i groups compared to the vehicle group (Fig. 7B). Notably, the pGSK3 β (Ser 9)/total GSK3 β ratio in the HIPP was significantly higher in the ND and SGLT2-i groups than in the vehicle group (Fig. 7C).

These findings indicate that the improvement in the peripheral insulin signaling induced by SGLT2-i and DPP4-i also positively affects the brain insulin signaling.

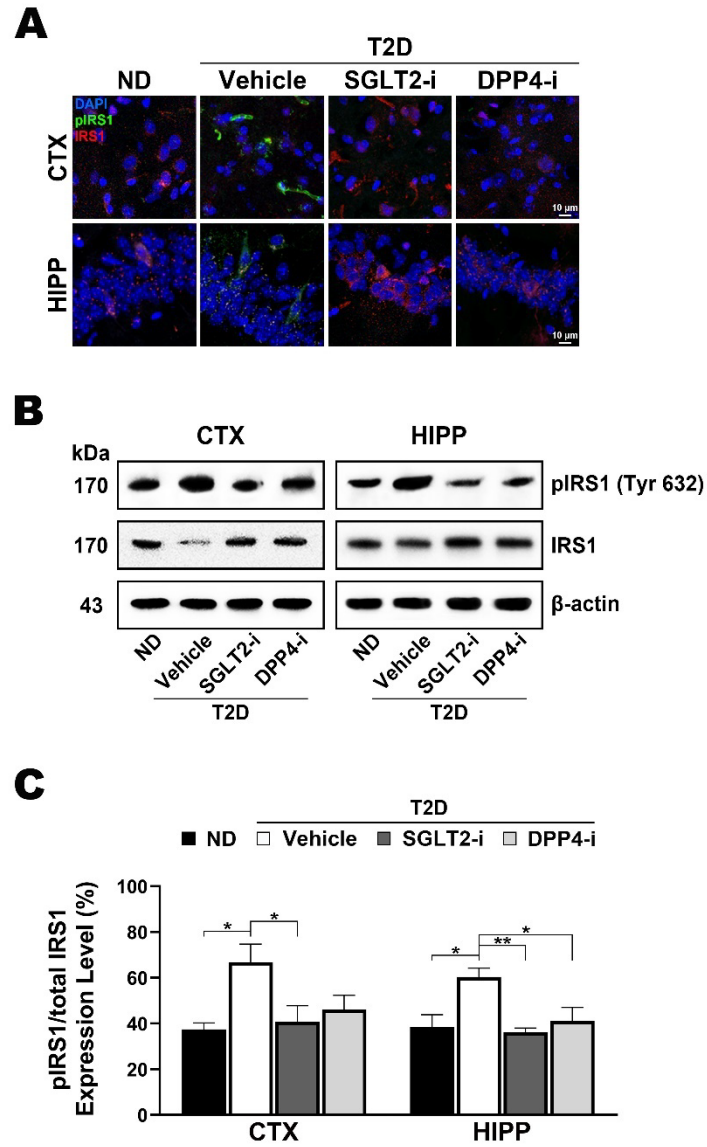


Figure 5. SGLT2-i and DPP4-i improved brain insulin signaling pathway: IRS1. (A) Representative IHC images of pIRS1 (Tyr 632) and IRS1. Scale bar = 10 μ m. (B) WB of pIRS1 (Tyr 632) and IRS1 with a size of 170 kDa. (C) The bar graph of the pIRS1 (Tyr 632)/total IRS1 (n = 3). β -actin served as a loading control. Data are presented as mean \pm S.E.M. * P < 0.05, ** P < 0.01.

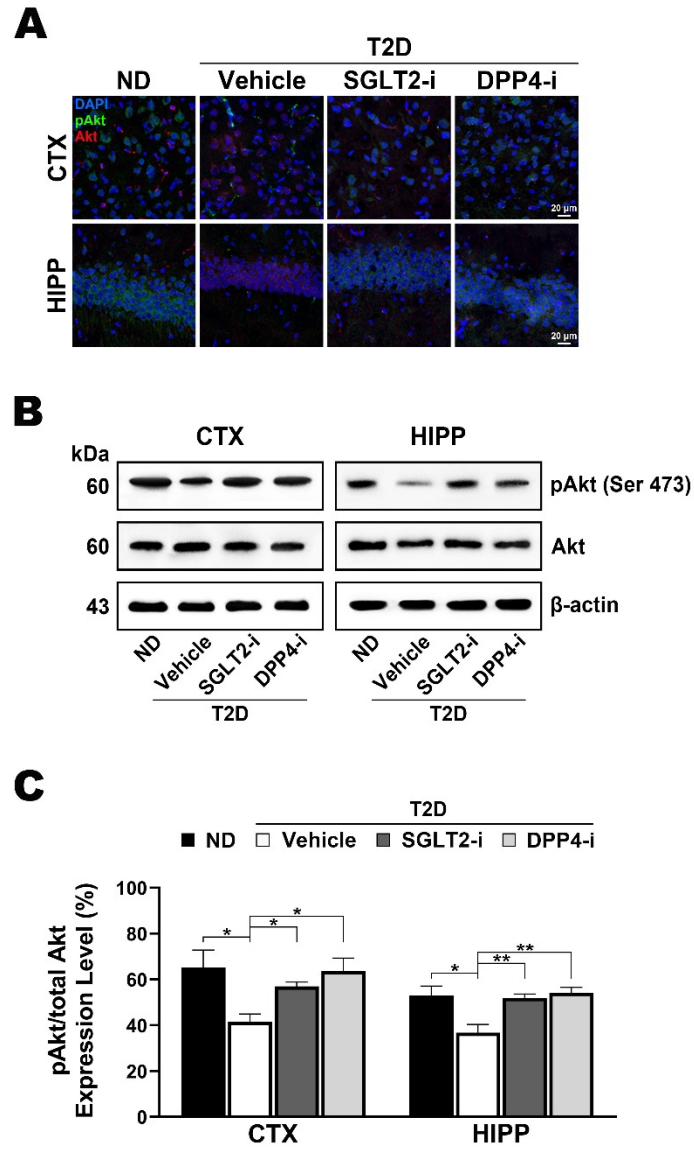


Figure 6. SGLT2-i and DPP4-i improved brain insulin signaling pathway: Akt. (A) Representative IHC images of pAkt (Ser 473) and Akt. Scale bar = 20 μ m. (B) WB of pAkt (Ser 473) and Akt with a size of 60 kDa. (C) The bar graph of the pAkt (Ser 473)/total Akt (n = 3). β -actin served as a loading control. Data are presented as mean \pm S.E.M. * P < 0.05, ** P < 0.01.

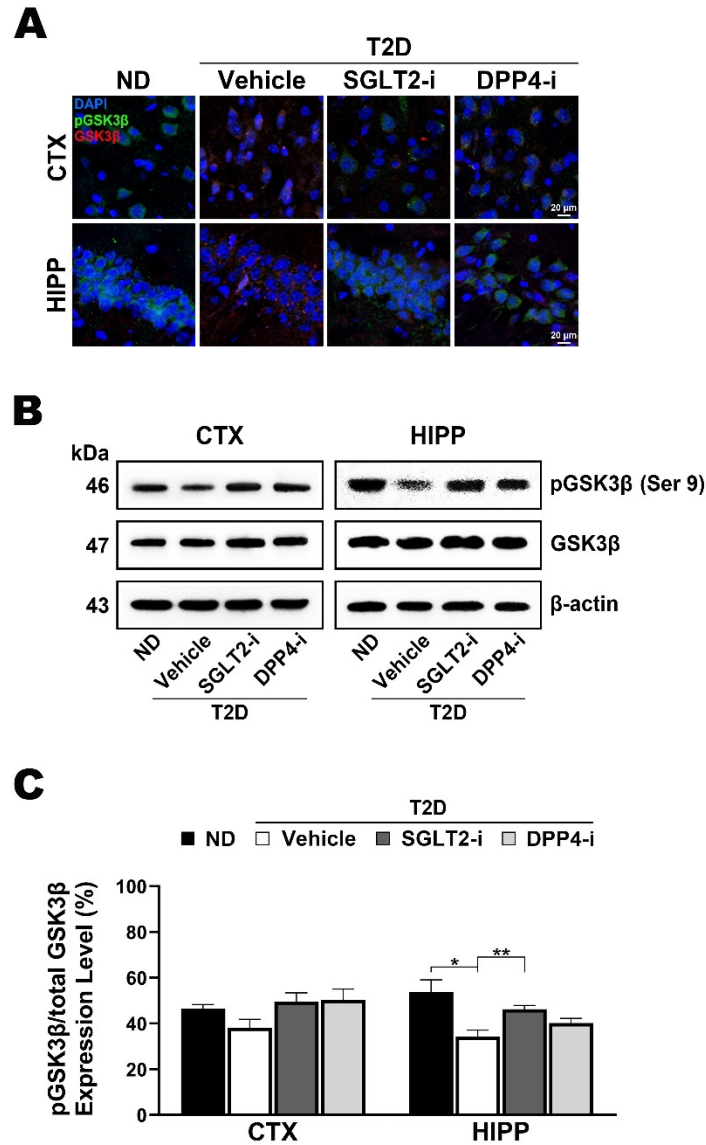


Figure 7. SGLT2-i and DPP4-i improved brain insulin signaling pathway: GSK3β. (A) Representative IHC images of pGSK3β (Ser 9) and GSK3β. Scale bar = 20 μm. (B) WB of pGSK3β (Ser 9) with a size of 46 kDa and GSK3β with a size of 47 kDa. (C) The bar graph of the pGSK3β (Ser 9)/total GSK3β (n = 3). β-actin served as a loading control. Data are presented as mean ± S.E.M. **P* < 0.05, ***P* < 0.01.

3.3. SGLT2-i and DPP4-i changed glucose utilization in the brain

Previously, it was confirmed that SGLT2-i and DPP4-i treatments restore both the peripheral and brain insulin signaling. The improvement in insulin signaling affects the brain glucose utilization.

The ^{18}F -FDG-PET scanning is an important imaging technique used to visualize *in vivo* metabolic activity.^{24,25} It is primarily used for the diagnosis and evaluation of conditions such as cancer, neurological disorders, and cardiovascular diseases.

Glucose utilization in the mice was assessed using the ^{18}F -FDG-PET imaging at week 19, examining transverse, coronal, and sagittal sections (Fig. 8A). Quantitative evaluation of ^{18}F -FDG uptake in the brain regions from sagittal images revealed no significant differences between the ND and vehicle groups. However, compared to the vehicle group, the SGLT2-i and DPP4-i groups showed significantly decreased the glucose uptake rates (Fig. 8B).

Contrary to the ^{18}F -FDG-PET results, the findings regarding GLUTs expression showed a different pattern. In the CTX and HIPP, the expression levels of GLUT1 with a size of 45 kDa, GLUT3 with a size of 48 kDa, and GLUT4 with a size of 55 kDa decreased in the vehicle group (Fig. 9A). Quantitative analysis showed that the ratios of GLUT1/ β -actin, GLUT3/ β -actin, and GLUT4/ β -actin were significantly reduced in the vehicle group compared to other groups, particularly in the HIPP (Fig. 9B-D).

Typically, GLUTs expression and the ^{18}F -FDG-PET patterns are correlated, with decreased GLUTs expression in AD brains being associated with reduced glucose metabolism as observed in the ^{18}F -FDG-PET scanning.²⁶ Similar phenomena can occur in T2D brains. However, in this study, the patterns of GLUTs expression and the ^{18}F -FDG-PET did not follow the typical tendencies.

Combining these results, it can be concluded that insulin signaling was restored through SGLT2-i and DPP4-i treatments, leading to increased GLUTs expression at the cellular level and thereby enhancing glucose uptake. However, the significantly higher glucose uptake rate in the vehicle group compared to the SGLT2-i and DPP4-i groups suggests that the glucose not absorbed by cells was reflected in the ^{18}F -FDG-PET imaging.

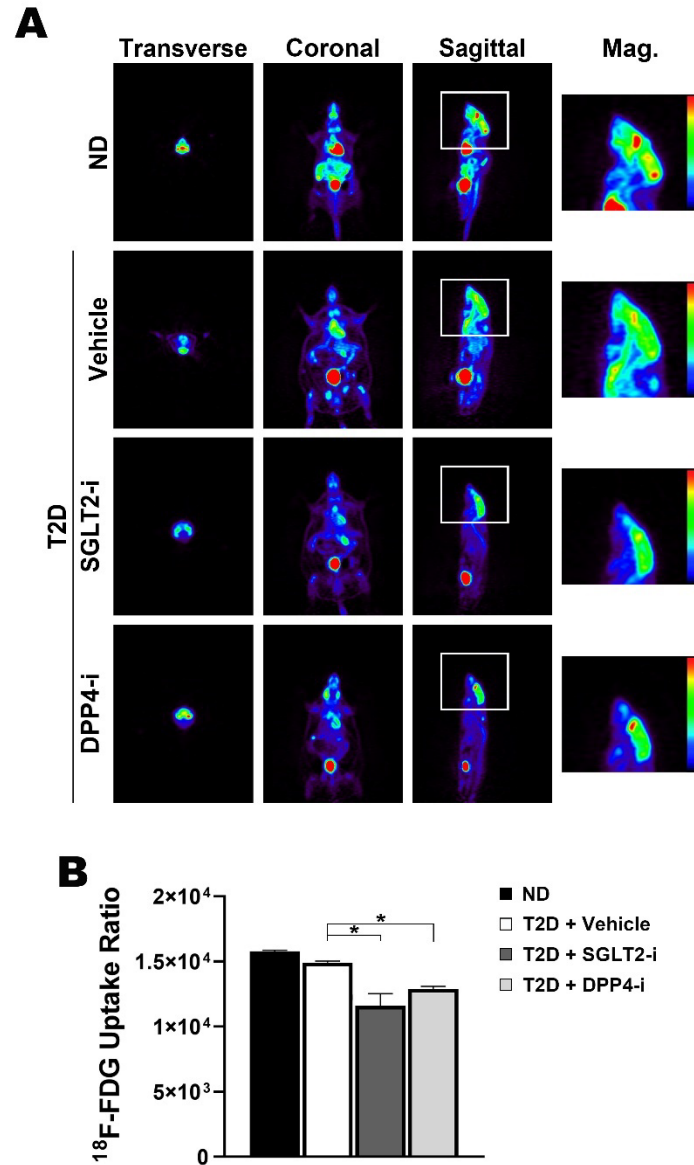


Figure 8. SGLT2-i and DPP4-i altered brain glucose uptake. (A) Representative ¹⁸F-FDG-PET image. (B) The bar graph of ¹⁸F-FDG uptake ratio (n = 4). Data are presented as mean ± S.E.M. **P* < 0.05.

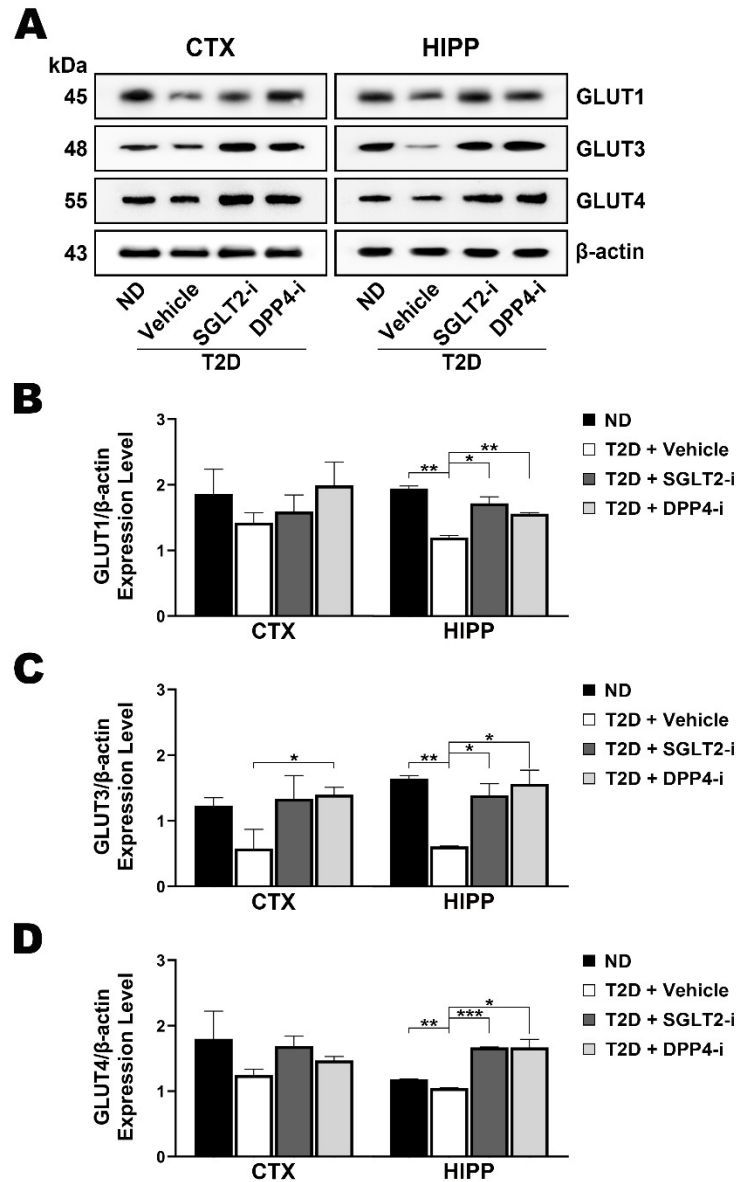


Figure 9. SGLT2-i and DPP4-i increased GLUTs. (A) WB of GLUT1 with a size of 45 kDa, GLUT3 with a size of 48 kDa and GLUT4 with a size of 55 kDa. The bar graph of the (B) GLUT1/ β -actin ($n = 3$), (C) GLUT3/ β -actin ($n = 3$), (D) GLUT4/ β -actin ($n = 3$). β -actin served as a loading control. Data are presented as mean \pm S.E.M. * $P < 0.05$, ** $P < 0.01$, *** $P < 0.001$.

3.4. SGLT2-i and DPP4-i increased ketone metabolic in the brain

The brain primarily uses glucose as an energy source but can utilize ketone bodies when glucose is insufficient.²⁷ The observed decrease in ketone bodies in the brains of patients with AD and T2D suggests impaired energy metabolism in the brain. Insulin resistance may impede cerebral glucose utilization by brain cells, predisposing them to resort to ketone bodies as an alternative energy substrate. Decreased levels of ketone bodies, in conjunction with insulin resistance, could further exacerbate cerebral energy insufficiency.

Ketone bodies are produced in the liver through the breakdown of fatty acids and exist mainly as acetoacetate (AcAc), β -hydroxybutyrate (BHB), and acetone. In T2D patients, insulin resistance can impair fatty acid metabolism. Similarly, in AD patients, changes in metabolic pathways can reduce ketone body production. These factors combined can lead to lower levels of ketone bodies.²⁸

Ketone metabolism involves several key enzymes and transporters, including 3-hydroxy-3-methylglutaryl-CoA lyase (*HMGCL*), 3-hydroxy-3-methylglutaryl-CoA synthase 2 (*HMGCS2*), 3-hydroxybutyrate dehydrogenase 1 (*BDHI*), peroxisome proliferator-activated receptor α (*PPAR- α*), monocarboxylate transporter 1 (*MCT1*), *MCT2*, sodium-coupled monocarboxylate transporter 1 (*SMCT1*), and *SMCT2*.

To investigate the effects of SGLT2-i and DPP4-i on brain ketone metabolism, the qPCR analysis was performed. The vehicle group showed significantly reduced the mRNA levels of *HMGCL*, *HMGCS2*, *BDHI*, *PPAR- α* , *MCT1*, *MCT2*, *SMCT1*, and *SMCT2* compared to the ND group. In contrast, the SGLT2-i group exhibited a significant increase in the mRNA levels of all these markers, except *SMCT1*, compared to the vehicle group. The DPP4-i group showed significant increases in *HMGCS2*, *PPAR- α* , *MCT1*, *MCT2*, and *SMCT2* mRNA levels compared to the vehicle group (Fig. 10).

The alterations induced by SGLT2-i and DPP4-i in glucose utilization and ketone bodies suggests that the potential of ketone bodies to function as an alternative energy source alongside glucose. This is particularly beneficial in insulin-resistant conditions, helping to mitigate the brain's energy deficit. Therefore, these findings indicate that SGLT2-i and DPP4-i can promote the use of both glucose and ketone bodies in the brain, providing metabolically beneficial effects and supporting the brain's energy requirements.

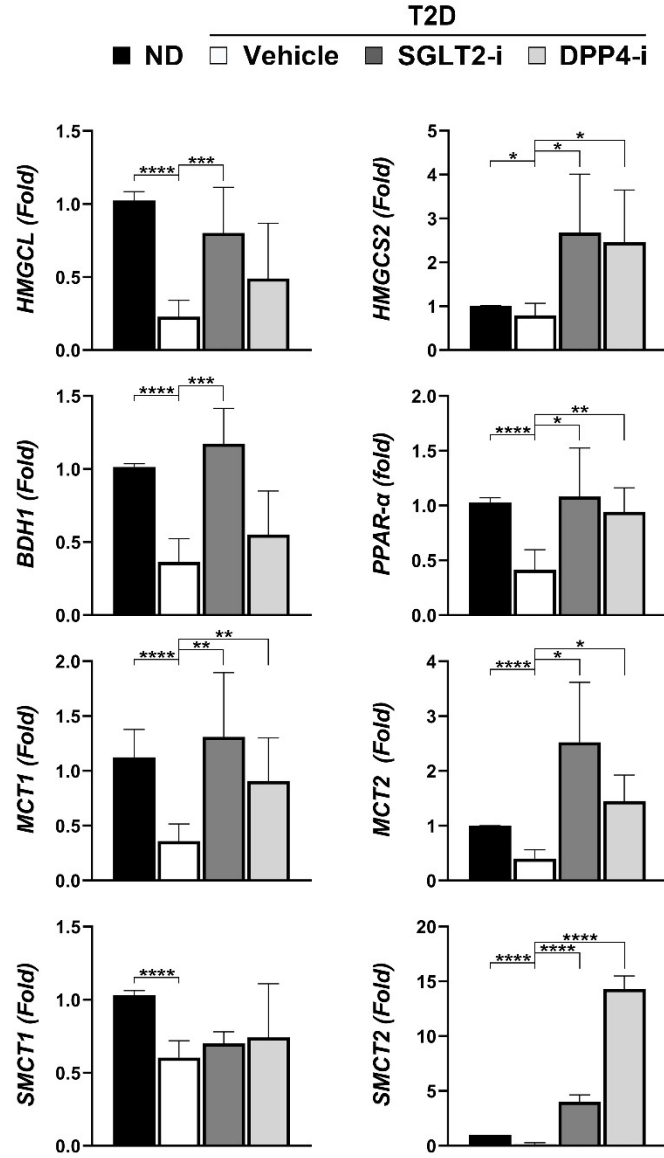


Figure 10. SGLT2-i and DPP4-i affected brain ketone metabolism. The bar graph of the qPCR evaluating *HMGCL*, *HMGCS2*, *BDHI*, *PPAR-α*, *MCT1*, *MCT2*, *SMCT1* and *SMCT2* ($n = 3$). 18S rRNA was used as an internal control for normalization. Data are presented as mean \pm S.E.M. * $P < 0.05$, ** $P < 0.01$, *** $P < 0.001$ **** $P < 0.0001$.

3.5. SGLT2-i and DPP4-i improved hippocampal-dependent cognitive functions

To assess the impact of SGLT2-i and DPP4-i on learning and memory abilities in mice, the NORT and MWM were conducted.

The NORT is based on the tendency of mice to show interest in novel objects over familiar ones, enabling the assessment of object recognition ability and memory. The test is conducted over three days, consisting of habituation, training, and probe test (Fig. 11A). On the training day, identical objects were placed in quadrant 1 (Q1) and Q4, and during the probe test, the original object in Q4 was replaced with a novel object to observe the behavior of the mice (Fig. 11B). The ND, SGLT2-i, and DPP4-i groups exhibited paths where they spent more time in the area with the novel object compared to the vehicle group (Fig. 11C). Measuring the time spent by the mice in Q1 and Q4 revealed a significant reduction in the time spent in Q4 by the vehicle group compared to the ND group (Fig. 11D). Additionally, there was a substantial difference in the time taken to explore the novel object among the ND, SGLT2-i, and DPP4-i groups compared to the vehicle group (Fig. 11E). The discrimination index, which is calculated as the ratio of the time spent exploring the novel object to the total time spent exploring both objects, is used to assess learning ability, with a score above 60% indicating normal learning capacity. The discrimination index graph showed a significant decrease in the vehicle group compared to the ND group, while the SGLT2-i and DPP4-i groups showed a significant increase compared to the vehicle group (Fig. 11F).

The MWM was conducted over six days to assess spatial learning and memory in mice by having them locate a hidden platform (Fig. 12A). During the training period, the platform was positioned between the E and N, and it was removed for the probe test (Fig. 12C). Throughout the training period, a progressive decrease in the time taken by the mice to find the platform was observed in the ND, SGLT2-i, and DPP4-i groups (Fig. 12B). During the probe test, the behavior of the mice in the pool was monitored for 90 seconds, revealing that the vehicle group exhibited paths that did not remain in the vicinity of the platform location compared to the other groups (Fig. 12D). The time spent and the number of crossings over the platform location during the probe test were reduced in the vehicle group compared to the ND group, whereas the SGLT2-i and DPP4-i groups showed a significant increase relative to the vehicle group (Fig. 12E, F).

Furthermore, the latency to reach the platform location from the starting point was longest in the vehicle group, showing significant differences from the ND, SGLT2-i, and DPP4-i groups (Fig. 12G).

These results suggest that both SGLT2-i and DPP4-i enhance cognitive function in the T2D-AD mouse model.

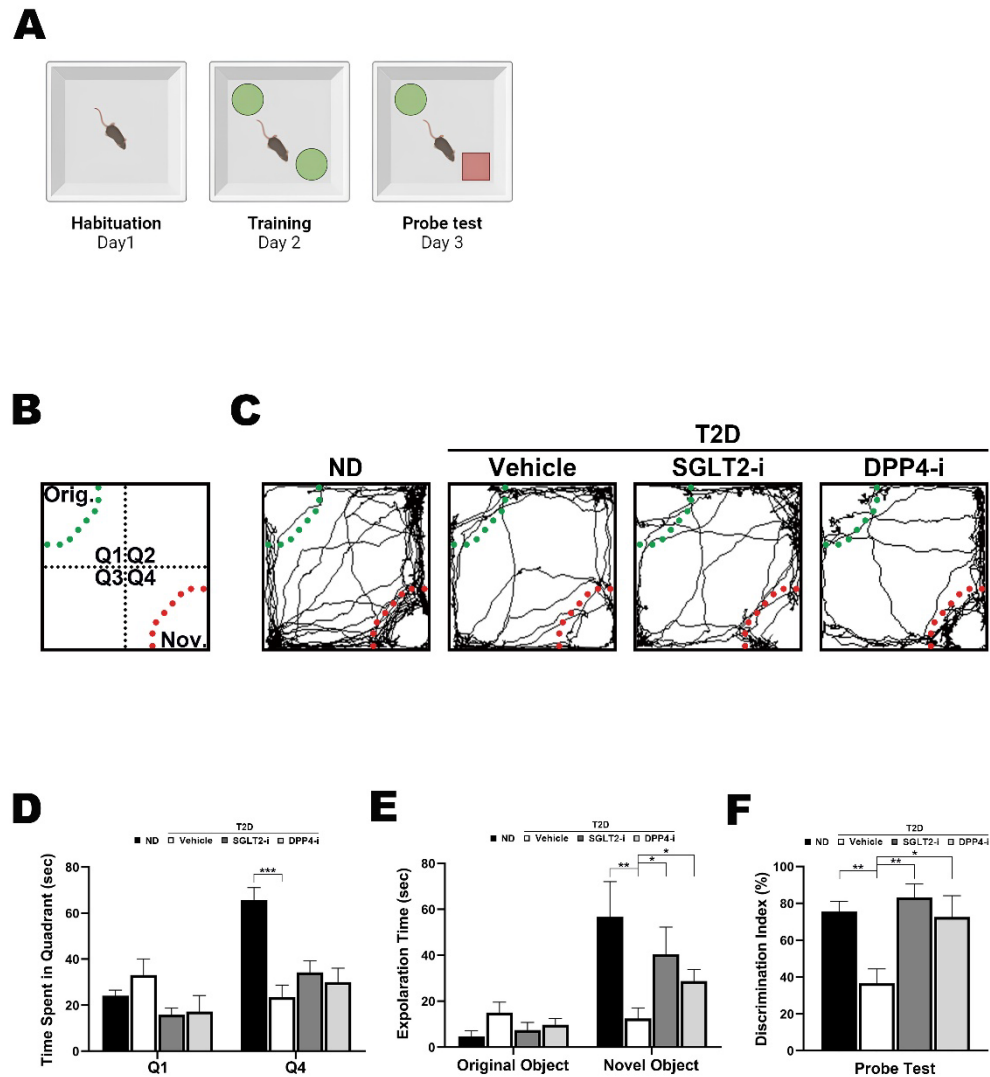


Figure 11. SGLT2-i and DPP4-i improved learning and memory functions: NORT. (A) Method of the NORT. (B) Diagram of the arena. (C) Paths taken by the mice during 5 minutes of the probe test ($n = 8$). (D) Time spent by the mice in Q1 and Q4 during the probe test ($n = 8$). (E) Time spent by the mice on original and novel objects during the probe test ($n = 8$). (F) Index of time to explore novel object compared to time to explore all objects ($n = 8$). Data are presented as mean \pm S.E.M. * $P < 0.05$, ** $P < 0.01$, *** $P < 0.001$.

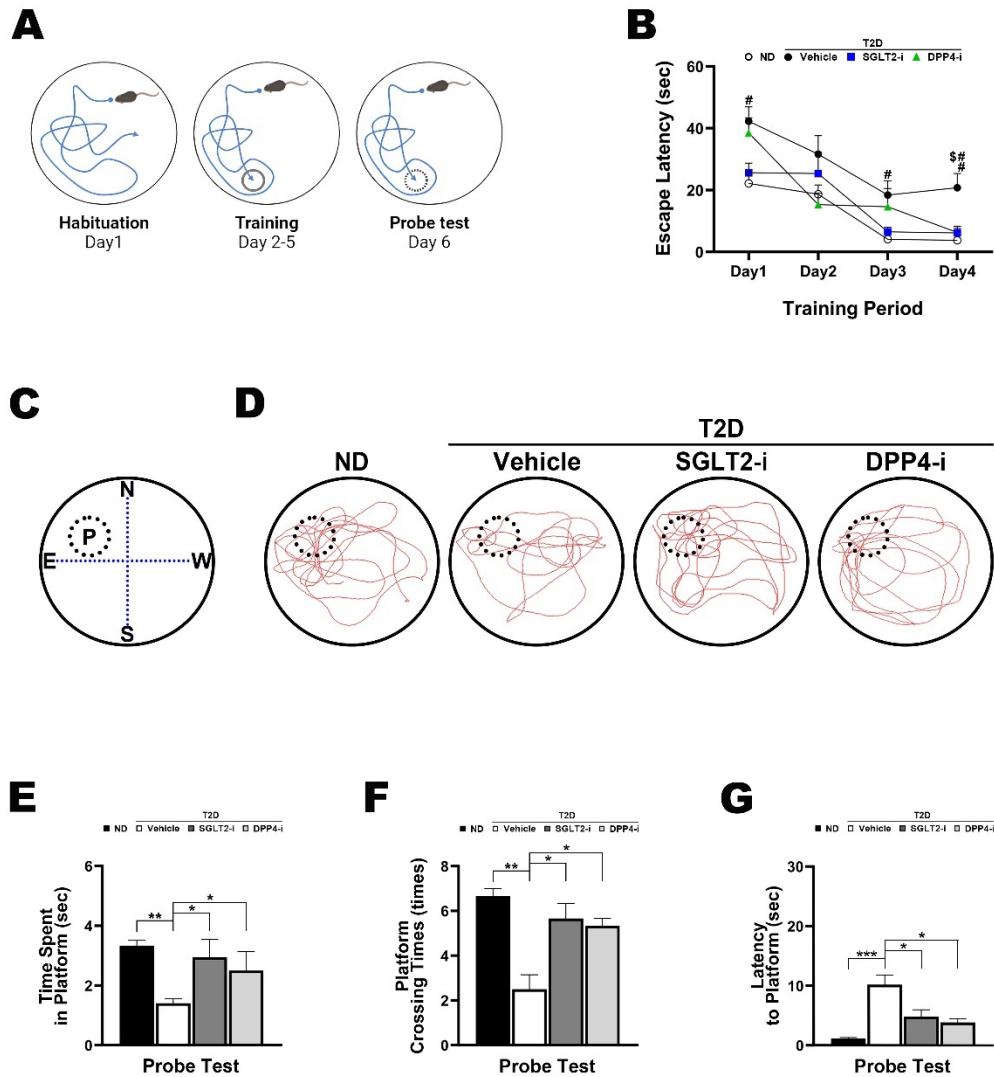


Figure 12. SGLT2-i and DPP4-i improved learning and memory functions: MWM. (A) Method of the MWM. (B) Changes in time taken by the mice to find the platform during the training period (n = 8). (C) Diagram of the pool. (D) Paths taken by the mice during the 90-second probe test (n = 8). (E) Time spent by the mice to locate the area where the platform was located during the probe test (n = 8). (F) Number of times mice crossed the area where the platform was located (n = 8). (G) Time taken by the mice to reach the area where the platform was located from the starting point (n

= 8). Data are presented as mean \pm S.E.M. #, $P < 0.05$, ##, $P < 0.01$ compared with the vehicle and SGLT2-i or DPP4-i groups. * $P < 0.05$, ** $P < 0.01$, *** $P < 0.001$.

3.6. SGLT2-i and DPP4-i reduced pTau and A β accumulation in the brain

Regulation of the IRS1/Akt/GSK3 β insulin signaling pathway can influence tau phosphorylation in the brain. GSK3 β exists in active and inactive forms depending on its phosphorylation state, and phosphorylation of GSK3 β by pAkt is known to inhibit and inactivate GSK3 β .^{7,29,30} The active form of GSK3 β phosphorylates tau at most serine and threonine residues, increases A β accumulation, and promotes A β -mediated neuronal apoptosis.³¹ To investigate the neuroprotective effects of SGLT2-i and DPP4-i, tau hyperphosphorylation and A β accumulation in the CTX and HIPP was evaluated.

In the IHC analysis, pTau (Thr 231) was stained with FITC, and tau was stained with rhodamine. In the vehicle group, the FITC-stained pTau (Thr 231) signal was stronger than the rhodamine-stained tau signal. Furthermore, the pTau fluorescence intensity was lower in the ND, SGLT2-i, and DPP4-i groups compared to the vehicle group (Fig. 13A). Additionally, the expression level of pTau (Thr 231) with a size of 46 kDa in both the CTX and HIPP was increased in the vehicle group compared to the other groups (Fig. 13B). The pTau (Thr 231)/total Tau ratio was significantly higher in the vehicle group compared to the ND group in both the CTX and HIPP. Notably, the ratio in the HIPP was significantly reduced in the SGLT2-i and DPP4-i groups compared to the vehicle group (Fig. 13C).

Moreover, neurons were identified by staining A β and MAP2 with FITC and rhodamine, respectively. The fluorescence intensity of A β was highest in the CTX and HIPP of the vehicle group compared to the other groups. The fluorescence intensity of MAP2, a neuron-specific marker, was lower in the vehicle group compared to the other groups. This indicates that neurons were damaged in the vehicle group due to A β accumulation. In contrast, the ND, SGLT2-i, and DPP4-i groups exhibited lower A β fluorescence intensity and higher MAP2 fluorescence intensity (Fig. 14A). The WB results were consistent with the IHC findings (Fig. 14B). In both the CTX and HIPP, the A β / β -actin ratio was significantly increased in the vehicle group compared to the ND group. The DPP4-i group showed a significant reduction in the A β / β -actin ratio compared to the vehicle group (Fig. 14C).

Taken together, these results suggest that SGLT2-i is effective in reducing pTau, while DPP4-i is effective in reducing A β , particularly in the HIPP. These findings imply that SGLT2-i and

DPP4-i modulate tau phosphorylation and A β accumulation through different mechanisms in the brain.

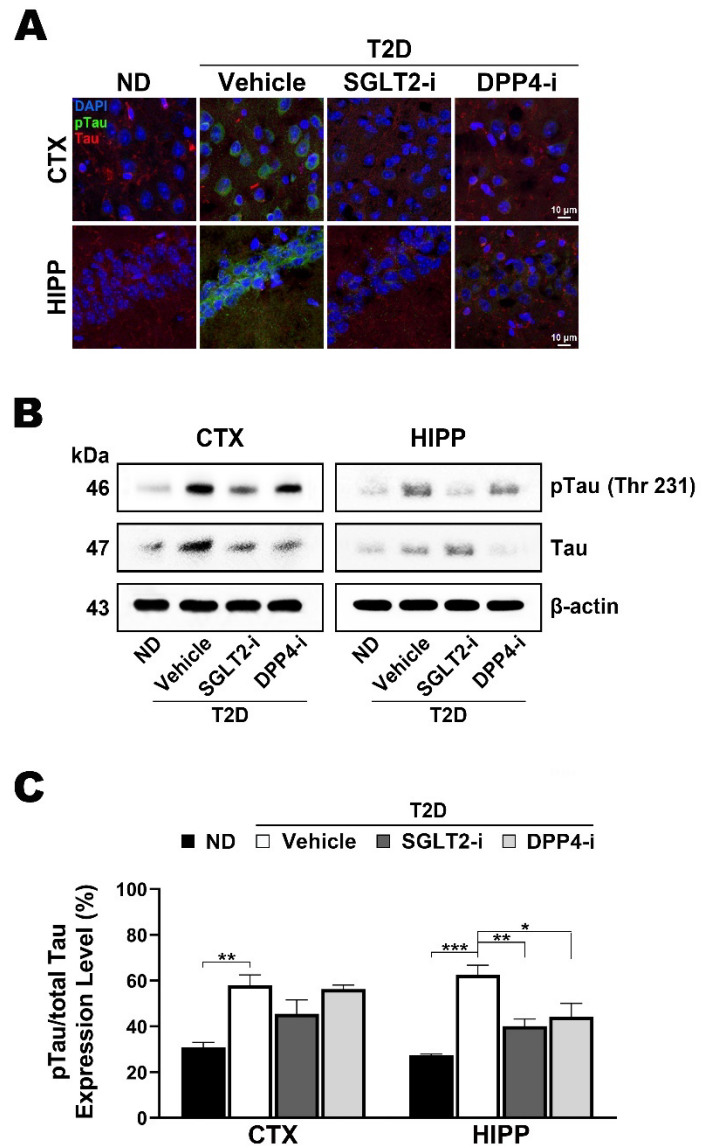


Figure 13. SGLT2-i and DPP4-i regulated tau phosphorylation. (A) Representative IHC images of pTau (Thr 231) and Tau. Scale bar = 10 μ m. (B) WB of pTau (Thr 231) with the size of 46 kDa and Tau with the size of 47 kDa. (C) The bar graph of the pTau (Thr 231)/total Tau (n = 3). β -actin served as a loading control. Data are presented as mean \pm S.E.M. * P < 0.05, ** P < 0.01, *** P < 0.001.

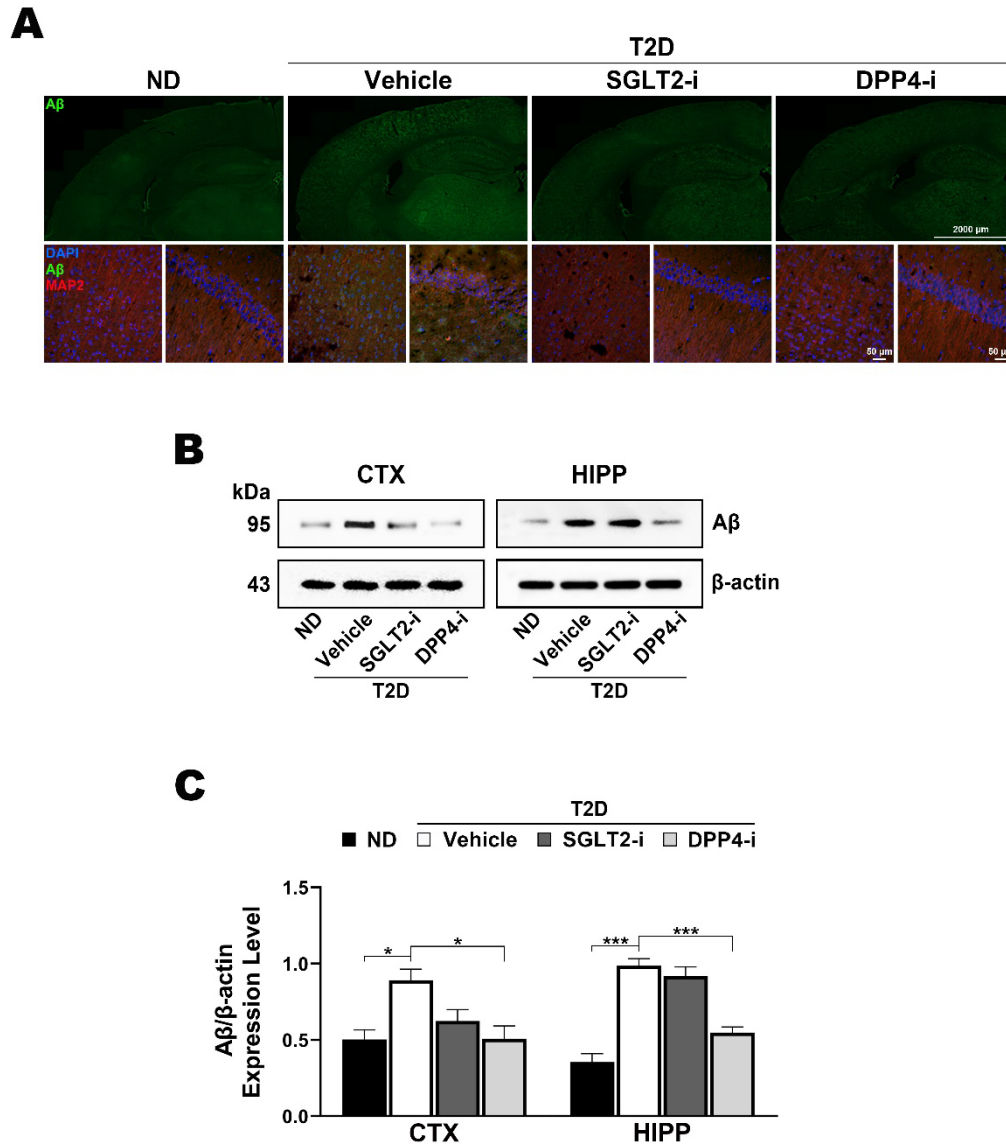


Figure 14. SGLT2-i and DPP4-i reduced A β accumulation. (A) Representative IHC images of A β . Scale bar = 2000 μ m (A β), 50 μ m (MERGE). (B) WB of A β with the size of 95 kDa. (C) The bar graph of A β / β -actin (n = 3). β -actin served as a loading control. Data are presented as mean \pm S.E.M. * P < 0.05, *** P < 0.001.

3.7. SGLT2-i reduced pTau level by activating ACE2/Ang (1-7)/

MasR, whereas DPP4-i decreased A β accumulation by increasing IDE level

While both SGLT2-i and DPP4-i enhanced cognitive function in the T2D-AD mouse model, the differential effects on pTau and A β reduction suggest that these drugs improve cognition through distinct mechanisms.

The renin-angiotensin system (RAS) is a hormonal system in the body that regulates blood pressure and electrolyte homeostasis, and it is also present in the brain.^{32,33} Various components of the RAS in the brain are associated with neuroprotection and cognitive function. In the RAS, Ang I is converted to Ang II by ACE1, which binds to Ang II receptor type 1 (AT1R) to induce vasoconstriction, inflammatory responses, and insulin resistance. Conversely, when Ang I is converted to Ang (1-7) by ACE2, the ACE2/Ang (1-7)/MasR axis counteracts the effects of the Ang II/AT1R axis. SGLT2-i is known to modulate the RAS and activate MasR.³⁴ Therefore, It was hypothesized that SGLT2-i could restore insulin signaling and reduce tau phosphorylation through MasR of the RAS.

In the IHC analysis, MasR was stained with FITC and MAP2 was stained with rhodamine. The signal intensity of MasR stained with FITC was more pronounced in the ND, SGLT2-i, and DPP4-i groups compared to the vehicle group in both the CTX and HIP (Fig. 15A). The WB analysis revealed a decrease in the expression level of ACE2 with a size of 120 kDa protein in the vehicle group compared to other groups (Fig. 15B). The ACE2/ β -actin ratio indicated a significant reduction in ACE2 expression in the vehicle group in both the CTX and HIP. In contrast, ACE2 expression significantly increased in the ND, SGLT2-i, and DPP4-i groups compared to the vehicle group (Fig. 15C). Additionally, the expression level of MasR with a size of 50 kDa was reduced in the vehicle group compared to the ND, SGLT2-i, and DPP4-i groups in both the CTX and HIP (Fig. 15B). The MasR/ β -actin ratio demonstrated a significant decrease in MasR expression in the vehicle group compared to the ND group in both the CTX and HIP. In the CTX, both the SGLT2-i and DPP4-i groups showed significant differences compared to the vehicle group, whereas in the HIP, only the SGLT2-i group showed a significant difference from the vehicle group (Fig. 15D).

Additionally, IDE is generally known for its role in degrading or clearing insulin, but in AD, A β also serves as a substrate for IDE.³⁵ Hyperinsulinemia due to insulin resistance can increase A β through competition between insulin and A β for IDE. Considering the previous findings that A β expression decreased in the DPP4-i group, it was posited that the improvement in insulin signaling due to DPP4-i would ultimately enhance IDE binding to A β , thereby promoting A β degradation.

In the IHC analysis, IDE was stained with FITC and MAP2 was stained with rhodamine. The FITC-stained IDE signal intensity was reduced in the vehicle group compared to other groups in both the CTX and HIPP (Fig. 16A). Furthermore, the WB results showed a decrease in the expression level of IDE with a size of 118 kDa in the vehicle group compared to other groups in both the CTX and HIPP (Fig. 16B). In the CTX, the IDE/ β -actin ratio was significantly reduced in the vehicle group compared to the ND group, while it significantly increased in the SGLT2-i and DPP4-i groups compared to the vehicle group. In the HIPP, only the DPP4-i group showed a significant difference compared to the vehicle group (Fig. 16C).

These results indicated that both SGLT2-i and DPP4-i groups exhibited effectiveness in the CTX compared to the vehicle group. However, differences were observed between the SGLT2-i and DPP4-i in the HIPP, suggesting that SGLT2-i and DPP4-i enhance cognitive function through different mechanisms.

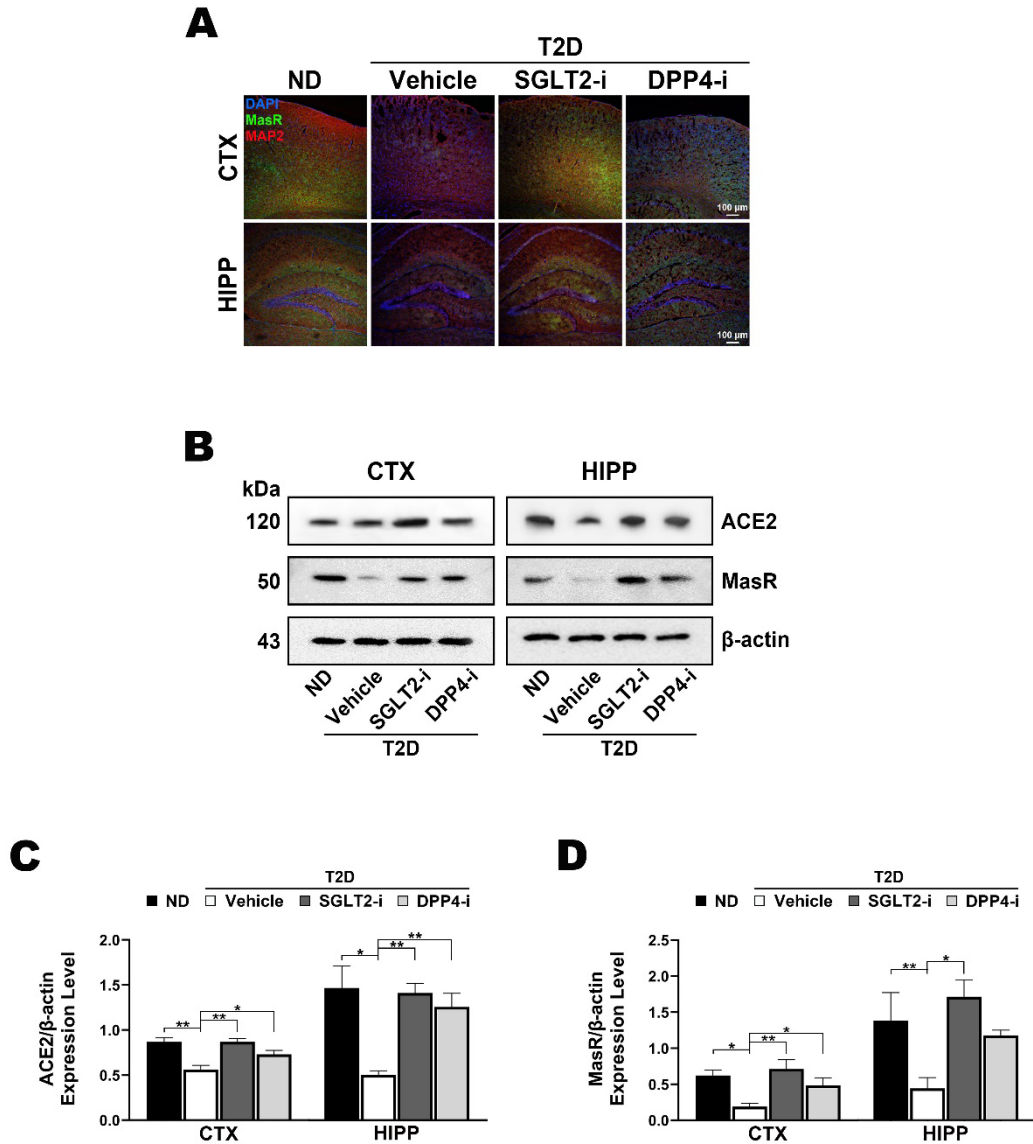


Figure 15. SGLT2-i reduced tau phosphorylation by activating ACE2/Ang (1-7)/MasR. (A) Representative IHC images of MasR and MAP2. Scale bar = 100 μ m. (B) WB of ACE2 with a size of 120 kDa and MasR with a size of 50 kDa. The bar graph of the (C) ACE2/ β -actin ($n = 3$) and (D) MasR/ β -actin ($n = 3$). β -actin served as a loading control. Data are presented as mean \pm S.E.M. * $P < 0.05$, ** $P < 0.01$.

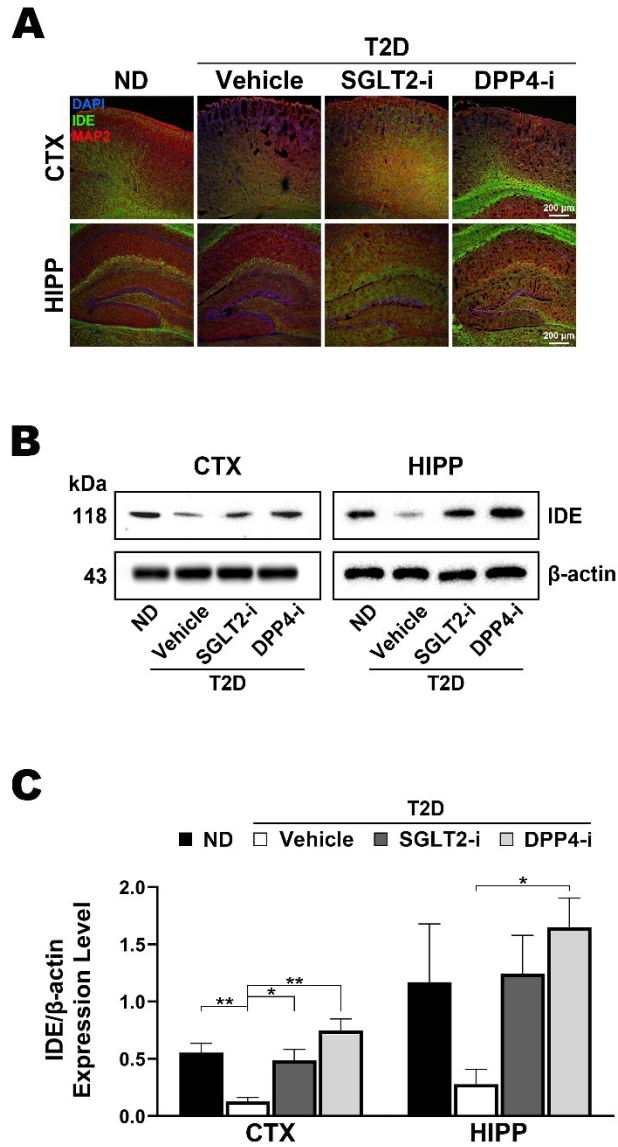


Figure 16. DPP4-i reduced A β accumulation by increasing IDE level. (A) Representative IHC images of IDE and MAP2. Scale bar = 200 μ m. (B) WB of IDE with a size of 118 kDa. (C) The bar graph of the IDE/ β -actin (n = 3). β -actin served as a loading control. Data are presented as mean \pm S.E.M. * P < 0.05, ** P < 0.01.

Part 2. Brain metabolic changes caused by SGLT2-i and DPP4-i influenced brain inflammatory responses

SGLT2-i and DPP4-i were confirmed to improve cognitive function by enhancing the brain insulin signaling, glucose utilization, and ketone bodies. Recent studies have reported that ketone regulation through SGLT2-i and DPP4-i promotes polarization of macrophages to from a pro-inflammatory phenotype (M1) to an anti-inflammatory phenotype (M2) by reducing the production of pro-inflammatory cytokines.²¹

This indicates that the increase in ketone bodies due to SGLT2-i and DPP4-i not only affects neuronal metabolism but also influences the activity of the brain immune cells, microglia.

Therefore, in this part, it was investigated that the effects of SGLT2-i and DPP4-i-induced microglial activation on pTau and A β .

3.8. SGLT2-i and DPP4-i reduced pro-inflammatory cytokines in the brain

To confirm the activation of microglia induced by SGLT2-i and DPP4-i, TMEM119, a microglial marker was stained. The IHC analysis, TMEM119 was stained with FITC. Resting microglia have elongated branches and small cell bodies, whereas activated microglia have enlarged cell bodies and shortened branches.³⁶ The phenotype of the FITC-stained TMEM119 in the ND, SGLT2-i, and DPP4-i groups resembled that of resting microglia, while the phenotype of TMEM119 in the vehicle group indicated a rounded morphology characteristic of activated microglia (Fig. 17). These results suggest that the increase in ketone bodies due to SGLT2-i and DPP4-i affects microglial activity.

To further investigate the decrease in pro-inflammatory cytokine production in the SGLT2-i and DPP4-i groups, the cytokine array was performed to determine the expression levels of various cytokines. The transparency overlay template facilitated the identification of the locations where each cytokine was expressed (Fig. 18A). The cytokine array results revealed the expression of multiple cytokines in the vehicle, SGLT2-i, and DPP4-i groups (Fig. 18B). Among them, the expression levels of six cytokines, including CD54, interferon γ (IFN- γ), IL-16, colony stimulating factor 1 (M-CSF), C-X-C motif chemokine 12 (CXCL12), and tissue inhibitor matrix

metalloproteinase 1 (TIMP-1), were significantly higher in the vehicle group compared to other groups, particularly CD54, IL-16, and M-CSF, which were significantly increased compared to the ND group (Fig. 18C). Additionally, IL-1 β , a representative pro-inflammatory cytokine, and IL-4, a representative anti-inflammatory cytokine, were examined. The WB analysis showed that the expression level of IL-4 with a size of 20 kDa was decreased in the vehicle group compared to other groups, while IL-1 β with a size of 17 kDa was increased in the vehicle group compared to other groups (Fig. 19A). The IL-4/ β -actin ratio demonstrated a decrease in IL-4 expression in both the CTX and HIPP of the vehicle group (Fig. 19B). Furthermore, the IL-1 β / β -actin ratio showed a significant increase in IL-1 β expression in the vehicle group compared to the ND group in both the CTX and HIPP (Fig. 19C).

These results suggest that SGLT2-i and DPP4-i reduce the expression of pro-inflammatory cytokines and increase the expression of anti-inflammatory cytokines, leading to changes in microglial activity.

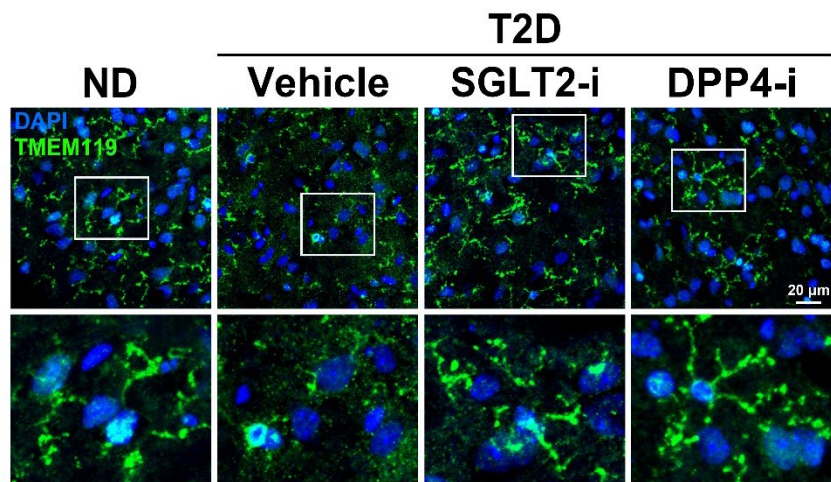


Figure 17. SGLT2-i and DPP4-i altered microglial activity. Representative IHC images of TMEM119. Scale bar = 20 μm.

A

	1	2	3	4	5	6	7	8	9	10	11	12	13	14	15	16	17	18	19	20	21	22	23	24
A	Reference																						Reference	
B	CXCL13	C5a	G-CSF	GM-CSF	CCL1	CCL11	CD54	IFN- γ	IL-1 α	IL-1 β	IL-1ra	IL-2												
C	IL-3	IL-4	IL-5	IL-6	IL-7	IL-10	IL-13	IL-12 p70	IL-16	IL-17	IL-23	IL-27												
D	CXCL10	CXCL11	CXCL1	M-CSF	CCL2	CCL12	CXCL9	CCL3	CCL4	CXCL2	CCL5	CXCL12												
E	CCL17	TIMP-1	TNF- α	TREM-1																				
F	Reference																							Negative

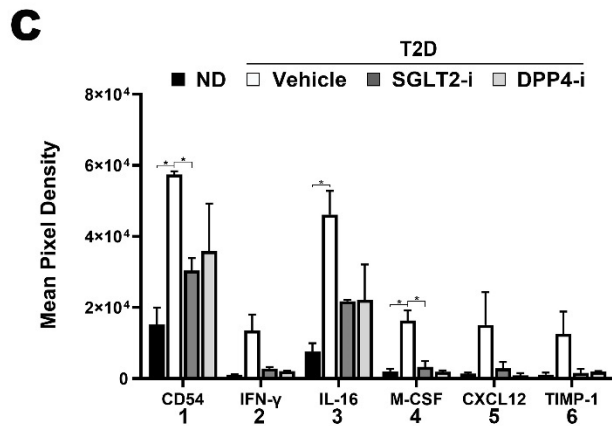
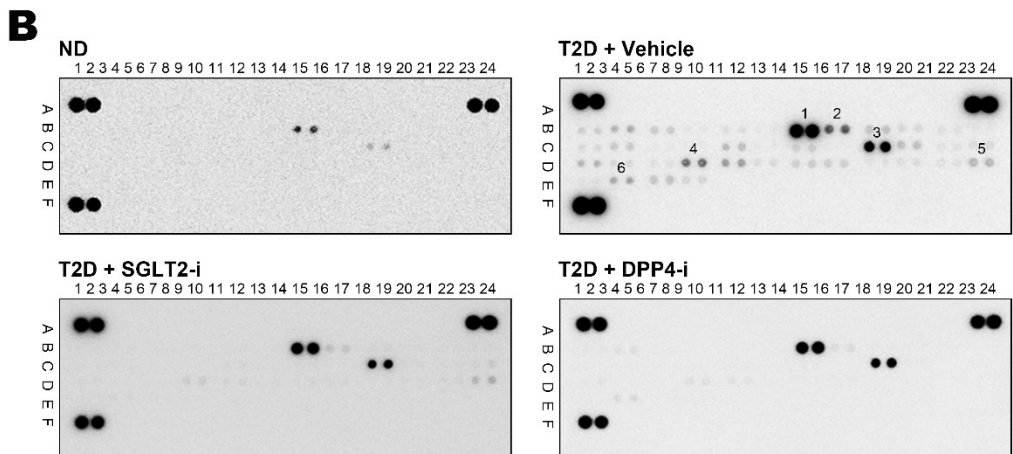


Figure 18. SGLT2-i and DPP4-i reduced anti-inflammatory cytokines. (A) The template of a mouse cytokines array. (B) Representative chemiluminescence images of a mouse cytokines array. (C) The bar graph of CD54, IFN- γ , IL-16, M-CSF, CXCL12 and TIMP-1 (n = 3). Data are presented as mean \pm S.E.M. * P < 0.05.

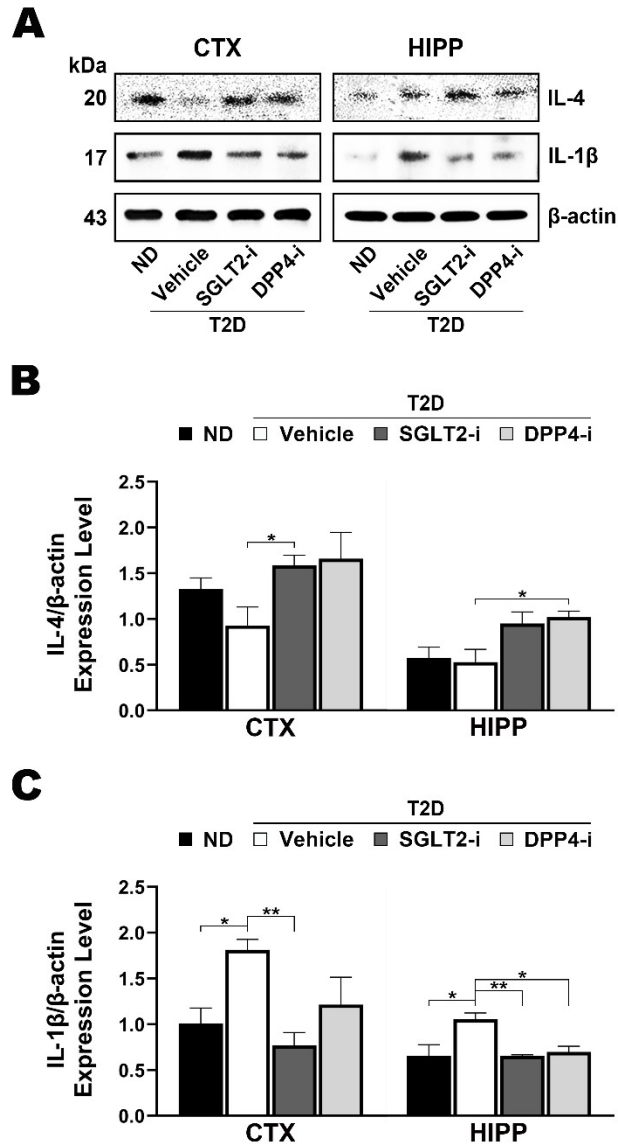


Figure 19. SGLT2-i and DPP4-i suppressed M1-induced cytokines and increased M2-induced cytokines. (A) WB of IL-4 with a size of 20 kDa and IL-1 β with a size of 17 kDa. The bar graph of the (B) IL-4/ β -actin (n = 3) and (C) IL-1 β / β -actin (n = 3). β -actin served as a loading control. Data are presented as mean \pm S.E.M. * P < 0.05, ** P < 0.01.

3.9. SGLT2-i and DPP4-i induced microglia to M2 phenotype

Cytokines induce phenotypic changes in microglia and play an important role in regulating their activity in various physiological and pathological conditions. The microglial phenotypes are broadly categorized into M1 and M2, each expressing different markers. Specifically, microglia in the M1 state typically express CD86, whereas those in the M2 state express CD206.³⁷

Accordingly, in the IHC analysis, CD206 was stained with FITC and CD86 was stained with rhodamine. Compared to other groups, the FITC fluorescence intensity of CD206 in the vehicle group was the lowest, while the rhodamine-stained CD86 in the vehicle showed the highest intensity (Fig. 20A). Additionally, the WB analysis results consistent with those obtained from the IHC analysis. In both the CTX and HIPP, the expression level of CD206 with a size of 180 kDa was reduced in the vehicle group compared to other groups, while the expression level of CD86 with a size of 70 kDa was increased (Fig. 20B). The CD206/ β -actin ratio showed significant differences between the ND and SGLT2-i groups compared to the vehicle group in the CTX, and between the SGLT2-i and DPP4-i groups compared to the vehicle group in the HIPP (Fig. 20C). The CD86/ β -actin ratio in the vehicle group was significantly higher in both the CTX and HIPP compared to the ND group. Furthermore, the SGLT2-i group showed significant differences compared to the vehicle group in both the CTX and HIPP, while the DPP4-i group exhibited significant differences only in the CTX compared to the vehicle group (Fig. 20D).

These experimental results demonstrate that SGLT2-i and DPP4-i reduce the expression of pro-inflammatory cytokines, leading to a conversion in microglial phenotype from M1 to M2.

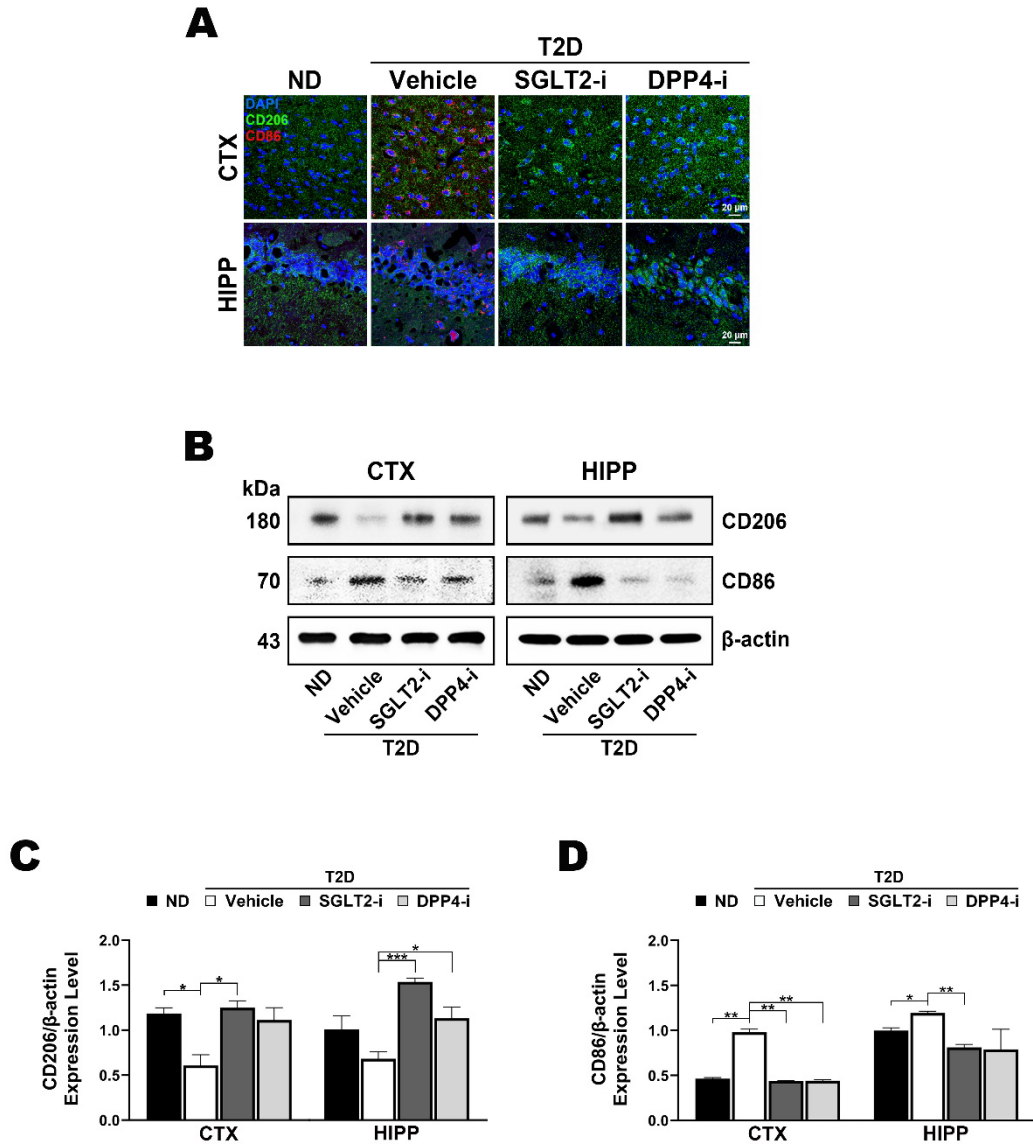


Figure 20. SGLT2-i and DPP4-i changed the phenotype of microglia. (A) Representative IHC images of CD86 and CD206. Scale bar = 20 μ m. (B) WB of CD206 with a size of 180 kDa and CD86 with a size of 70 kDa. The bar graph of the (C) CD206/ β -actin (n = 3) and (D) CD86/ β -actin (n = 3). β -actin served as a loading control. Data are presented as mean \pm S.E.M. * P < 0.05, ** P < 0.01, *** P < 0.001.

3.10. SGLT2-i and DPP4-i altered the phenotype of microglia by inhibiting NLRP3 inflammasome

The activation of NLRP3 inflammasome in microglia is involved in the induction of pro-inflammatory cytokines such as IL-1 β and IL-18. Chronic inflammation resulting from NLRP3 inflammasome activation leads to neurodegenerative diseases and neuronal damage through interactions with pTau and A β .³⁸ Therefore, inhibition of NLRP3 inflammasome is being investigated as a potential therapeutic strategy to reduce neuroinflammation induced by phosphorylation of tau proteins and A β accumulation. One of the ketone bodies, BHB, has been shown to inhibit NLRP3 inflammasome activation.³⁹

To confirm the activation of NLRP3 inflammasome in the T2D-AD mouse model, the IHC was performed. The signal intensity of NLRP3 inflammasome stained with FITC was markedly higher in the vehicle group compared to the ND, SGLT2-i, and DPP4-i groups (Fig. 21A). Additionally, to verify the expression of NLRP3 inflammasome in microglia, NLRP3 inflammasome and TMEM119 were stained with FITC and Alexa fluor 555, respectively. In the IHC analysis, the signal intensity of NLRP3 inflammasome was higher in the vehicle group and co-localization of NLRP3 inflammasome and TMEM119 was observed in the vehicle group (Fig. 21B). Furthermore, the expression level of NLRP3 inflammasome with a size of 118 kDa was significantly increased in both the CTX and HIP in the vehicle group (Fig. 21C). Particularly in the CTX, the NLRP3 inflammasome/ β -actin ratio was significantly elevated in the vehicle group compared to the ND, SGLT2-i, and DPP4-i groups (Fig. 21D).

In summary, these findings suggest that SGLT2-i and DPP4-i increase ketone bodies, which in turn inhibit NLRP3 inflammasome, reduce the secretion of pro-inflammatory cytokines, and promote the transition of microglia to M2.

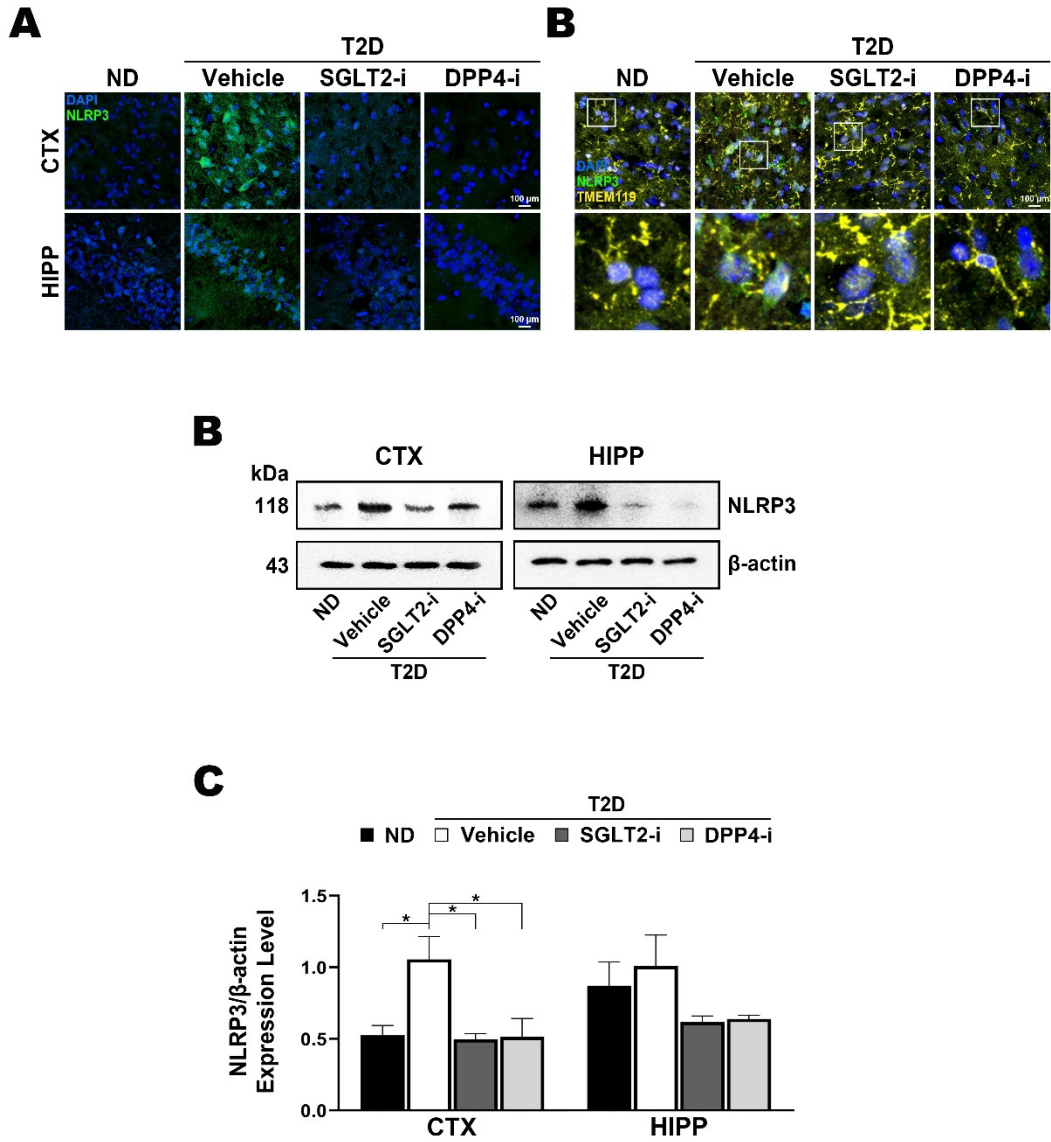


Figure 21. SGLT2-i and DPP4-i suppressed NLRP3 inflammasome activation. Representative IHC images of (A) NLRP3 inflammasome and (B) TMEM119. Scale bar = 100 μ m. (C) WB of NLRP3 inflammasome with a size of 118 kDa. (D) The bar graph of the NLRP3 inflammasome/ β -actin (n = 3). β -actin served as a loading control. Data are presented as mean \pm S.E.M. * P < 0.05.

3.11. SGLT2-i suppressed NLRP3 inflammasome by regulating the binding of pTau and CX3CR1, whereas DPP4-i suppressed NLRP3 inflammasome by regulating the binding of A β and TLR4

The release of pTau outside neurons, binding to microglial CX3CR1, activates NLRP3 inflammasome via the LC3 pathway, leading to the secretion of pro-inflammatory cytokines and induction of inflammatory responses.⁴⁰ Additionally, A β binding to TLR4 on microglia is known to activate NLRP3 inflammasome via the NF- κ B pathway, inducing inflammation.¹⁴

Previous findings revealed that SGLT2-i and DPP4-i reduce pTau and A β levels, respectively, while increasing ketone bodies and suppressing NLRP3 inflammasome activity. Consequently, it is hypothesized that the decreased pTau induced by SGLT2-i prevents its binding to microglial CX3CR1, thereby inhibiting NLRP3 inflammasome activation, while DPP4-i activates GLP-1R to suppress signaling through A β and TLR4.^{41,42}

The WB results showed increased the expression level of LC3 with a size of 18 kDa and 16 kDa in both the CTX and HIPPO of the vehicle group (Fig. 22A). The LC3/ β -actin ratio revealed a significant increase in the vehicle group compared to the ND and SGLT2-i groups (Fig. 22B). Moreover, the expression level of CX3CR1 with a size of 40 kDa increased in the CTX and HIPPO of the vehicle group (Fig. 22A), with the CX3CR1/ β -actin ratio significantly higher in the vehicle group than in the SGLT2-i and DPP4-i groups in the CTX and higher in all groups in the HIPPO (Fig. 22C).

Additionally, the expression level of NF- κ B with a size of 65 kDa increased in both the CTX and HIPPO of the vehicle group (Fig. 23A). Notably, the NF- κ B/ β -actin ratio was significantly higher in the vehicle group than in the ND and DPP4-i groups in the HIPPO (Fig. 23B). The expression level of GLP-1R with a size of 53 kDa decreased in both the CTX and HIPPO of the vehicle group (Fig. 23A), with a significantly lower the GLP-1R/ β -actin ratio in the vehicle group compared to all other groups in the HIPPO (Fig. 23C).

In summary, these results suggest that SGLT2-i inhibits NLRP3 inflammasome activation via pTau and CX3CR1, while DPP4-i is implicated in the suppression of NLRP3 inflammasome activation through A β and GLP-1R.

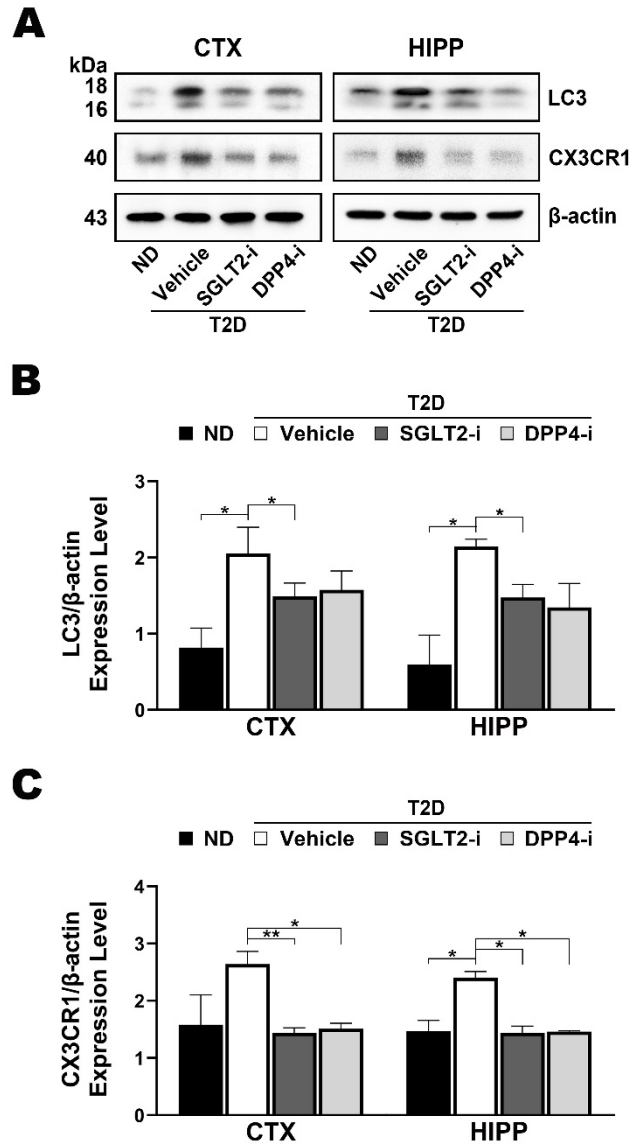


Figure 22. SGLT2-i suppressed NLRP3 inflammasome by regulating pTau and CX3CR1 binding. (A) WB of LC3 with a size of 18 kDa and 16 kDa and CX3CR1 with a size of 40 kDa. (B) The bar graph of the LC3/β-actin (n = 3). (C) The bar graph of the CX3CR1/β-actin (n = 3). β-actin served as a loading control. Data are presented as mean ± S.E.M. * $P < 0.05$, ** $P < 0.01$.

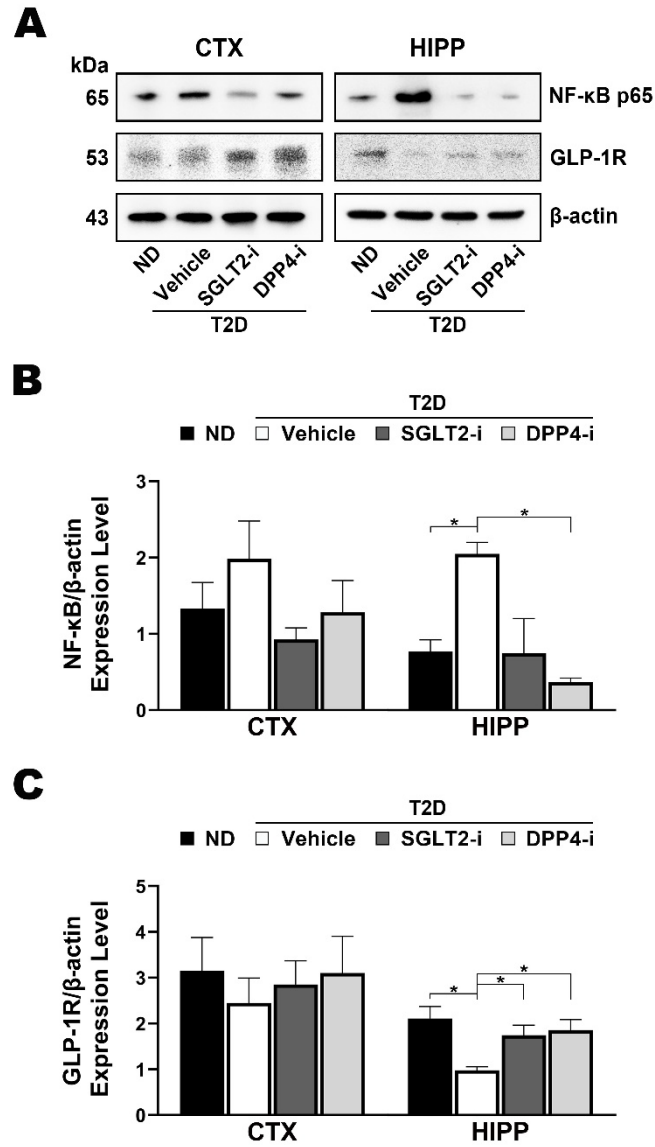


Figure 23. DPP4-i suppressed NLRP3 inflammasome by regulating A β and TLR4 binding. (A) WB of NF- κ B with a size of 65 kDa and GLP-1R with a size of 53 kDa. (B) The bar graph of the NF- κ B / β -actin (n = 3). (C) The bar graph of the GLP-1R/ β -actin (n = 3). β -actin served as a loading control. Data are presented as mean \pm S.E.M. * P < 0.05.

4. DISCUSSION

AD is a complex neurodegenerative disorder that remains incompletely understood. With emerging shared features between AD and T2D, their correlation is widely acknowledged. Indeed, diabetic patients are at higher risk for developing AD. However, studies on how diabetes influences the pathological processes of AD are relatively limited. Current treatments for AD primarily focus on symptom alleviation and have limited efficacy in fundamentally slowing or halting disease progression, highlighting the need for new therapeutic approaches.

SGLT2-i and DPP4-i, anti-diabetic drugs, have shown neuroprotective effects. However, the exact mechanisms remain unclear.

Therefore, this study aimed to elucidate the effects and mechanisms of SGLT2-i and DPP4-i in a T2D-AD mouse model. Through this study, a comprehensive approach was taken to understand the relationship between T2D and AD and to clarify the mechanisms underlying AD.

Firstly, this study demonstrated that inducing T2D-AD in mice through a 60% HFD and STZ administration, followed by treatment with SGLT2-i and DPP4-i, improved brain insulin signaling and induced metabolic changes in the brain.

Given that patients with T2D exhibit both insulin secretion dysfunction and insulin resistance, a mouse model was designed to more accurately mimic human conditions. Obesity is one of the major risk factors for T2D, which causes insulin resistance. Most current T2D animal models are obese. To induce obesity in mice, a 60% HFD was used.^{43,44} However, inducing T2D through diet alone is time-inefficient, so to accelerate disease progression and shorten the time required for model generation, STZ⁴⁵⁻⁴⁷, a glucosamine-nitrosourea compound that is selectively toxic to pancreatic β cells, was used to induce a hyperglycemic model. Along with the diet, a single low dose of STZ was administered IP, resulting in hyperglycemia associated with hyperinsulinemia and insulin resistance in the mice.⁴⁷⁻⁵⁰

Subsequently, SGLT2-i and DPP4-i reduced the BG and BW in the periphery, and the ITT and GTT showed that insulin resistance and glucose intolerance were alleviated in T2D. Further

investigation into the brain insulin signaling pathways revealed that the IRS1/Akt/GSK3 β signaling was improved, indicating that the enhancement of the peripheral insulin signaling also positively impacted the brain insulin signaling.

Furthermore, improvement in the brain insulin signaling led to metabolic changes in the brain, as observed through the ^{18}F -FDG-PET imaging. ^{18}F -FDG, a glucose analogue, is used as an indicator of glucose metabolism in the brain. Under normal physiological conditions, brain cells use glucose at relatively high rates for function and energy.⁵¹ However, in AD brains, the PET imaging using ^{18}F -FDG as a tracer shows reduced glucose utilization. Decreased glucose metabolism correlates with synaptic density and function, indicating that cognitive impairment is associated with brain glucose consumption. Additionally, reduced insulin responsiveness in T2D brains decreases the expression of important GLUTs, notably GLUT3 and GLUT4 in neurons, leading to a general reduction in ^{18}F -FDG uptake. However, the pattern of the brain ^{18}F -FDG uptake can vary depending on the stage and severity of diabetes.^{52,53}

In this study, the T2D-AD mice showed reduced the GLUTs expression, which increased upon drug administration, yet the ^{18}F -FDG-PET imaging revealed decreased ^{18}F -FDG uptake with SGLT2-i and DPP4-i. The peripheral hyperglycemia in the T2D mice likely increases glucose concentration in the brain. Studies have shown that increased blood glucose enhances ^{18}F -FDG uptake in tissues. Additionally, reduced peripheral blood glucose with SGLT2-i and DPP4-i resulted in decreased ^{18}F -FDG uptake, although the GLUTs expression did not decrease, indicating differences in glucose uptake into cells compared to T2D. The fasting duration, different half-lives of SGLT2-i and DPP4-i, and other factors affecting ^{18}F -FDG absorption and clearance may have influenced these results, suggesting the need for further studies on fasting and drug administration timing and dosage.

The brain ketone bodies serve as alternative energy sources to glucose for organs such as the brain, muscles, and liver. Individuals with good metabolic health in these organs efficiently use ketone bodies for energy. The brain uses both glucose and ketone bodies as the primary energy sources, but impaired utilization of either can lead to decreased brain function.⁵⁴ Ketogenesis, the metabolic pathway generating ketone bodies, primarily occurs in the liver as follows: free fatty acids (FFA) undergo β -oxidation in the mitochondria to form acetyl-CoA,

which is then converted by HMGCS2 into 3-hydroxy-3-methylglutaryl-CoA (HMG-CoA), subsequently cleaved by HMG-CoA lyase to form AcAc. AcAc is reduced to β -hydroxybutyrate (β -OHB) by BDH1, released into the circulation by MCT1. β -OHB enters muscle mitochondria through MCT1 and MCT2, is reconverted to AcAc by BDH1, and transformed into acetoacetyl-CoA by succinyl-CoA. This is further converted into two acetyl-CoA molecules by mitochondrial acetoacetyl-CoA thiolase, entering the tricarboxylic acid (TCA) cycle to produce ATP.⁵⁵ Ketogenesis is sensitive to various hormonal stimuli released under physiological and pathological stress, with insulin being the most significant. Insulin decreases lipolysis and hepatic ketogenesis flux.⁵⁶

The fact that SGLT2-i and DPP4-i improve glucose utilization while also increasing the levels of ketone bodies suggests that ketone bodies can serve as an alternative energy source alongside glucose. This could help mitigate brain energy deficits, particularly in insulin-resistant states. Moreover, microglia can utilize ketone bodies to suppress the NF- κ B signaling, reduce pro-inflammatory enzymes such as cyclooxygenase-2 (Cox2) and inducible nitric oxide synthase (iNOS) and cytokines such as IL-6, tumor necrosis factor (TNF), and inhibit the NLRP3 inflammasome complex, thus exhibiting anti-inflammatory properties.⁵⁷ Therefore, increased ketone bodies from SGLT2-i and DPP4-i may promote anti-inflammatory effects in microglia, a topic that will be further elaborated upon later.

Secondly, this study demonstrated that while both SGLT2-i and DPP4-i improve cognitive function, they do so through different mechanisms involving AD-related proteins.

It was confirmed that SGLT2-i and DPP4-i effectively reduce pTau and A β , respectively, leading to improvements in learning and memory abilities. The distinct mechanisms of SGLT2-i and DPP4-i appear to differentially affect pTau and A β , respectively, as elucidated in this study.

The RAS serves as a major hormonal system for regulating blood pressure and electrolyte balance, with implications for cognitive functions such as memory and mood regulation.⁵⁸ This system operates through various enzymatic reactions. Renin, secreted from juxtaglomerular cells in the kidney, is stimulated by factors such as decreased sodium concentration, lowered blood pressure, and reduced renal perfusion, leading to the conversion of angiotensinogen, generated in the liver by renin, into Ang I.⁵⁹ Ang I is then directly converted into Ang II by ACE1. Ang II

binds to AT1R, inducing vasoconstriction, stimulating aldosterone secretion, and promoting antidiuretic hormone secretion, ultimately leading to increased blood pressure and fluid retention.⁶⁰⁻⁶³ Moreover, it is known to contribute to inflammatory responses and the development of insulin resistance. Ang I can directly generate Ang (1-7) via ACE2. Additionally, Ang I can be initially converted into Ang II by ACE1 and subsequently converted into Ang (1-7) by ACE2. Ang (1-7) plays roles in vasodilation, lowering blood pressure, and exerting anti-inflammatory effects.⁶⁴ It binds to MasR, stimulating proteins involved in insulin signaling pathways and ameliorating the negative effects of Ang II.⁶⁵

Recent studies have demonstrated that anti-diabetic medications affect the RAS and MasR pathways, leading to anti-inflammatory effects and improvements in cardiovascular diseases. Particularly, SGLT2-i has been shown to regulate renin activity by reducing reabsorption of sodium and water in the kidneys, thus modulating aldosterone secretion involved in electrolyte balance, and even influencing the decrease of Ang II or the activation of MasR.^{66,67} Such the RAS modulation can occur not only peripherally but also within the central nervous system (CNS), where the ACE2/Ang (1-7)/MasR signaling pathway has been found to exert vascular and neuroprotective effects by regulating the ACE/Ang II/AT1R axis.

Therefore, it has been hypothesized that SGLT2-i can restore the brain insulin signaling by modulating the ACE2/Ang (1-7)/MasR axis. Furthermore, the ACE2 expression is assumed to be crucial for SGLT2-i to activate the RAS, with a positive correlation observed in the investigation of the ACE2 expression levels. Additionally, an increase in the MasR expression levels has been confirmed. These findings suggest that SGLT2 inhibitor therapy may ameliorate metabolic dementia, improve brain insulin signaling via the RAS, and the enhanced insulin signaling may inhibit abnormal phosphorylation of tau proteins.

IDE is known to play a significant role in the breakdown and clearance of insulin within the body.^{68,69} Improved insulin resistance through DPP4-i may facilitate efficient insulin degradation, potentially increasing the necessity and activity of IDE. As insulin signaling is restored, tissue sensitivity to insulin receptors increases, maintaining blood insulin levels at appropriate levels and regulating the amount of insulin IDE needs to process.^{70,71}

DPP4-i inhibits the degradation of GLP-1 and GIP, leading to increased serum concentrations of these hormones. GLP-1 exhibits neuroprotective effects in various tissues, including the brain,

and directly increases IDE expression and activity in the liver and muscle cells.²² Additionally, activation of GLP-1 receptors promotes the IDE gene expression via the cyclic adenosine monophosphate (cAMP)/protein kinase A (PKA) pathway. Elevated the IDE gene expression leads to metabolic pathway normalization, consequently increasing the amount of IDE required for the degradation of insulin and A β .^{17,72,73}

Therefore, it was assumed that DPP4-i increases the IDE expression within the brain, consequently influencing the degradation of A β . This assumption was confirmed by the observed increase in the IDE expression levels. These findings suggest that improved insulin resistance through DPP4-i leads to increased IDE expression and activity, influencing the degradation of A β . Moreover, enhanced insulin signaling in the brain may impact the regulation of APP metabolism, potentially promoting α -secretase activity, an enzyme involved in APP breakdown, thus inhibiting A β production.⁷⁴

Thirdly, this study demonstrated that SGLT2-i and DPP4-i reduce the production of pro-inflammatory cytokines in microglia and promote a conversion to M2.

Microglia, the immune cells of the CNS, play an important role in regulating neuroinflammatory responses and maintaining homeostasis by secreting various cytokines. Cytokines are proteins responsible for cell signaling, influencing inflammation, immune regulation, cell growth, and differentiation.⁷⁵⁻⁷⁷

The cytokine array results showed increased expression of CD54, IFN- γ , IL-16, M-CSF, CXCL12, and TIMP-1 in T2D mice, with significant elevations in CD54 and IL-16. However, SGLT2-i and DPP4-i reduced the overall expression of these cytokines. CD54, an intercellular adhesion molecule, facilitates immune cell adhesion and migration, promoting leukocyte recruitment and activation at inflammation sites.⁷⁸ IFN- γ , a potent pro-inflammatory cytokine, enhances the activation of macrophages and microglia, boosting antiviral and antitumor activities.⁷⁹ IL-16 induces chemotaxis of immune cells, including CD4⁺ T cells, and regulates immune responses, potentially playing a pro-inflammatory role under specific conditions.¹⁶ Conversely, M-CSF, CXCL12, and TIMP-1 exhibit anti-inflammatory properties, reflecting the complexity of inflammatory responses and physiological roles in T2D mice.

This study showed that SGLT2-i and DPP4-i decreased the expression of IL-1 β and increased the expression of IL-4, resulting in a conversion of microglia toward an M2. IL-1 β , a pro-inflammatory cytokine, promotes inflammation and immune cell activation, playing a key role in early inflammatory responses following neuronal injury.⁸⁰ IL-4, an anti-inflammatory cytokine, facilitates microglial differentiation towards inflammation suppression and tissue repair. Microglia activation to M1 or M2 is influenced by various stimuli.^{81,82} The observed reduction in IL-1 β and increase in IL-4 expression with SGLT2-i and DPP4-i treatment suggests that these drugs suppress inflammatory responses and promote anti-inflammatory cytokine and growth factor secretion by microglia, minimizing inflammatory damage and enhancing tissue regeneration.

Lastly, the anti-inflammatory effects in the brain induced by SGLT2-i and DPP4-i were shown to involve increased ketone bodies that reduce NLRP3 inflammasome activation in microglia, acting through different pathway.

Recent studies indicate that ketone bodies can modulate inflammation by inhibiting NLRP3 inflammasome activation in microglia.⁸³ NLRP3 inflammasome activation leads to the secretion of inflammatory cytokines IL-1 β and IL-18, promoting neuroinflammation. The activation of NLRP3 inflammasome is initiated by signals such as TLR or cytokine receptor activation, which activate the transcription factor NF- κ B, increasing the expression of NLRP3, pro-IL-1 β , and pro-IL-18.³⁸ Further activation signals from ATP, reactive oxygen species (ROS), or other stress signals promote NLRP3 inflammasome assembly. Activated NLRP3 protein binds with caspase recruitment domain (ASC) to form a large protein complex, activating caspase-1, which cleaves pro-IL-1 β and pro-IL-18 into their mature forms, subsequently secreted to enhance inflammation and signal surrounding cells. In microglia, NLRP3 inflammasome is closely associated with A β and tau proteins in neurodegenerative diseases such as AD.

Recent studies have revealed that a progressive increase in pTau occurs in parallel with an increase in CX3CR1.⁸⁴ One of the signaling pathways through which neurons and microglia communicate involves the neuronal cytokine C-X3-C motif ligand 1 (CX3CL1) and the microglial receptor CX3CR1. CX3CL1, expressed by neurons, can exist as a membrane-bound or secreted ligand. The binding of CX3CL1 to CX3CR1 keeps microglia in an "off" state,

suppressing the release of pro-inflammatory cytokines. In contrast, deficiency in either CX3CL1 or CX3CR1 leads to an increase in pro-inflammatory molecule production.⁸⁵ Although a correlation between neuroinflammation and tauopathy exists, with various studies indicating that microglia induce tau pathology and contribute to the spread of pathological tau, mechanistic evidence linking altered microglial activity to this pathology is sparse. It has been shown that extracellular tau binds to CX3CR1, increasing its internalization by microglia and competing with the natural ligand, CX3CL1, for binding to this receptor.

Therefore, the involvement of SGLT2-i in the reduction of the pTau and CX3CR1 expression was investigated. The results of this study confirm that SGLT2-i regulates CX3CR1 by suppressing the inflammatory response in microglia.

Additionally, A β signals through surface receptors on microglia such as TLR4 and triggering receptor expressed on myeloid cells 2 (TREM2) to promote NLRP3 inflammasome activation.¹⁴ TLR4, a receptor crucial for innate immune responses, recognizes pathogen-associated molecular patterns (PAMPs) and damage-associated molecular patterns (DAMPs).⁸⁶ Activation of TLR4 triggers the production of inflammatory cytokines by activating transcription factors like NF- κ B through myeloid differentiation primary response 88 (MyD88)-dependent and MyD88-independent pathways. The activation of GLP-1R by DPP4-i can suppress the expression of inflammatory cytokines, primarily by inhibiting transcription factors such as NF- κ B.

A hypothesis was proposed that the reduction of A β by DPP4-i is related to GLP-1R activation, and this was supported by confirming an increase in the GLP-1R expression.

These mechanisms suggest that SGLT2-i and DPP4-i may exert neuroprotective effects and play an important role in regulating inflammatory responses by modulating ketone bodies and altering microglial polarization.

This study had several limitations. The direct mechanism of action of SGLT2-i and DPP4-i in the brain has not been evaluated. Additionally, the combined effect of SGLT2-i and DPP4-i on AD has not been assessed. Although limited, the results of this study confirmed that SGLT2-i or DPP4-i improve learning and memory functions in T2D mice through distinct mechanisms.

In summary, the study indicates that anti-diabetic drugs can induce metabolic changes in neurons, including insulin signaling and glucose and ketone body regulation. These changes not only affect neurons but also influence microglial inflammation, suggesting that these drugs may provide a novel and effective strategy for treating and preventing brain diseases.

5. CONCLUSION

This study utilized the T2D-AD mouse model induced by a 60% HFD and STZ to demonstrate the effects of SGLT2-i and DPP4-i on improving the brain insulin signaling and metabolic changes. Administration of SGLT2-i and DPP4-i in the 60% HFD and STZ-induced mouse model ameliorated insulin resistance and glucose intolerance in both the peripheral tissues and brain, and improved the IRS1/Akt/GSK3 β pathway. SGLT2-i and DPP4-i respectively reduced phosphorylated tau and A β levels, thereby enhancing cognitive functions, and were shown to act through distinct mechanisms involving the RAS and IDE pathways. Additionally, SGLT2-i and DPP4-i promoted the conversion of microglia to M2 phenotype through increased ketone bodies and reduced the production of pro-inflammatory cytokines. SGLT2-i and DPP4-i acted to inhibit NLRP3 inflammasome via distinct mechanisms.

These findings indicate that anti-diabetic drugs can modulate insulin signaling and metabolic pathways in neurons and microglia, exerting neuroprotective and anti-inflammatory effects. Therefore, these results suggest that SGLT2-i and DPP4-i have the potential to mitigate neurodegenerative and inflammatory processes in T2D-AD. This provides a valuable basis for developing new therapeutic strategies beyond existing treatments.

REFERENCES

- 1 Arnold, S. E. *et al.* Brain insulin resistance in type 2 diabetes and Alzheimer disease: concepts and conundrums. *Nat Rev Neurol* **14**, 168-181, doi:10.1038/nrneurol.2017.185 (2018).
- 2 Breijyeh, Z. & Karaman, R. Comprehensive Review on Alzheimer's Disease: Causes and Treatment. *Molecules* **25**, doi:10.3390/molecules25245789 (2020).
- 3 Olsen, I. Porphyromonas gingivalis-Induced Neuroinflammation in Alzheimer's Disease. *Front Neurosci* **15**, 691016, doi:10.3389/fnins.2021.691016 (2021).
- 4 Chow, V. W., Mattson, M. P., Wong, P. C. & Gleichmann, M. An overview of APP processing enzymes and products. *Neuromolecular Med* **12**, 1-12, doi:10.1007/s12017-009-8104-z (2010).
- 5 Hur, J. Y. γ -Secretase in Alzheimer's disease. *Exp Mol Med* **54**, 433-446, doi:10.1038/s12276-022-00754-8 (2022).
- 6 Avila, J., Lucas, J. J., Perez, M. & Hernandez, F. Role of tau protein in both physiological and pathological conditions. *Physiol Rev* **84**, 361-384, doi:10.1152/physrev.00024.2003 (2004).
- 7 Avila, J. *et al.* Tau Phosphorylation by GSK3 in Different Conditions. *Int J Alzheimers Dis* **2012**, 578373, doi:10.1155/2012/578373 (2012).
- 8 Zhang, B., Lin, L., Wu, S. & Al-Masqari, Z. Multiple Subtypes of Alzheimer's Disease Base on Brain Atrophy Pattern. *Brain Sci* **11**, doi:10.3390/brainsci11020278 (2021).
- 9 Chatterjee, S. & Mudher, A. Alzheimer's Disease and Type 2 Diabetes: A Critical Assessment of the Shared Pathological Traits. *Front Neurosci* **12**, 383, doi:10.3389/fnins.2018.00383 (2018).
- 10 Galicia-Garcia, U. *et al.* Pathophysiology of Type 2 Diabetes Mellitus. *Int J Mol Sci* **21**, doi:10.3390/ijms21176275 (2020).
- 11 van der Heide, L. P., Ramakers, G. M. & Smidt, M. P. Insulin signaling in the central nervous system: learning to survive. *Prog Neurobiol* **79**, 205-221, doi:10.1016/j.pneurobio.2006.06.003 (2006).
- 12 Nguyen, T. T., Ta, Q. T. H., Nguyen, T. K. O., Nguyen, T. T. D. & Giau, V. V. Type 3

- Diabetes and Its Role Implications in Alzheimer's Disease. *Int J Mol Sci* **21**, doi:10.3390/ijms21093165 (2020).
- 13 Kellar, D. & Craft, S. Brain insulin resistance in Alzheimer's disease and related disorders: mechanisms and therapeutic approaches. *Lancet Neurol* **19**, 758-766, doi:10.1016/s1474-4422(20)30231-3 (2020).
- 14 Yang, J., Wise, L. & Fukuchi, K. I. TLR4 Cross-Talk With NLRP3 Inflammasome and Complement Signaling Pathways in Alzheimer's Disease. *Front Immunol* **11**, 724, doi:10.3389/fimmu.2020.00724 (2020).
- 15 Halle, A. *et al.* The NALP3 inflammasome is involved in the innate immune response to amyloid-beta. *Nat Immunol* **9**, 857-865, doi:10.1038/ni.1636 (2008).
- 16 Muzio, L., Viotti, A. & Martino, G. Microglia in Neuroinflammation and Neurodegeneration: From Understanding to Therapy. *Front Neurosci* **15**, 742065, doi:10.3389/fnins.2021.742065 (2021).
- 17 Sim, A. Y., Barua, S., Kim, J. Y., Lee, Y. H. & Lee, J. E. Role of DPP-4 and SGLT2 Inhibitors Connected to Alzheimer Disease in Type 2 Diabetes Mellitus. *Front Neurosci* **15**, 708547, doi:10.3389/fnins.2021.708547 (2021).
- 18 Berlanga-Acosta, J. *et al.* Insulin Resistance at the Crossroad of Alzheimer Disease Pathology: A Review. *Front Endocrinol (Lausanne)* **11**, 560375, doi:10.3389/fendo.2020.560375 (2020).
- 19 Deacon, C. F. A review of dipeptidyl peptidase-4 inhibitors. Hot topics from randomized controlled trials. *Diabetes Obes Metab* **20 Suppl 1**, 34-46, doi:10.1111/dom.13135 (2018).
- 20 Herat, L. Y. *et al.* SGLT2 Inhibitor-Induced Sympathoinhibition: A Novel Mechanism for Cardiorenal Protection. *JACC Basic Transl Sci* **5**, 169-179, doi:10.1016/j.jacbts.2019.11.007 (2020).
- 21 Kim, S. R. *et al.* SGLT2 inhibition modulates NLRP3 inflammasome activity via ketones and insulin in diabetes with cardiovascular disease. *Nat Commun* **11**, 2127, doi:10.1038/s41467-020-15983-6 (2020).
- 22 Ikeda, Y., Nagase, N., Tsuji, A., Kitagishi, Y. & Matsuda, S. Neuroprotection by dipeptidyl-peptidase-4 inhibitors and glucagon-like peptide-1 analogs via the modulation of AKT-signaling pathway in Alzheimer's disease. *World J Biol Chem* **12**, 104-113, doi:10.4331/wjbc.v12.i6.104 (2021).

- 23 Fajardo, R. J., Karim, L., Calley, V. I. & Bouxsein, M. L. A review of rodent models of type 2 diabetic skeletal fragility. *J Bone Miner Res* **29**, 1025-1040, doi:10.1002/jbmr.2210 (2014).
- 24 Bouter, C. *et al.* (18)F-FDG-PET Detects Drastic Changes in Brain Metabolism in the Tg4-42 Model of Alzheimer's Disease. *Front Aging Neurosci* **10**, 425, doi:10.3389/fnagi.2018.00425 (2018).
- 25 Bouter, C. & Bouter, Y. (18)F-FDG-PET in Mouse Models of Alzheimer's Disease. *Front Med (Lausanne)* **6**, 71, doi:10.3389/fmed.2019.00071 (2019).
- 26 Kyrтата, N., Emsley, H. C. A., Sparasci, O., Parkes, L. M. & Dickie, B. R. A Systematic Review of Glucose Transport Alterations in Alzheimer's Disease. *Front Neurosci* **15**, 626636, doi:10.3389/fnins.2021.626636 (2021).
- 27 Kapogiannis, D. & Avgerinos, K. I. Brain glucose and ketone utilization in brain aging and neurodegenerative diseases. *Int Rev Neurobiol* **154**, 79-110, doi:10.1016/bs.irm.2020.03.015 (2020).
- 28 Fukao, T., Lopaschuk, G. D. & Mitchell, G. A. Pathways and control of ketone body metabolism: on the fringe of lipid biochemistry. *Prostaglandins Leukot Essent Fatty Acids* **70**, 243-251, doi:10.1016/j.plefa.2003.11.001 (2004).
- 29 Lauretti, E., Dincer, O. & Praticò, D. Glycogen synthase kinase-3 signaling in Alzheimer's disease. *Biochim Biophys Acta Mol Cell Res* **1867**, 118664, doi:10.1016/j.bbamcr.2020.118664 (2020).
- 30 Neddens, J. *et al.* Phosphorylation of different tau sites during progression of Alzheimer's disease. *Acta Neuropathol Commun* **6**, 52, doi:10.1186/s40478-018-0557-6 (2018).
- 31 Hooper, C., Killick, R. & Lovestone, S. The GSK3 hypothesis of Alzheimer's disease. *J Neurochem* **104**, 1433-1439, doi:10.1111/j.1471-4159.2007.05194.x (2008).
- 32 Gravandi, M. M. *et al.* Therapeutic targeting of Ras/Raf/MAPK pathway by natural products: A systematic and mechanistic approach for neurodegeneration. *Phytomedicine* **115**, 154821, doi:10.1016/j.phymed.2023.154821 (2023).
- 33 Dominici, F. P., Burghi, V., Muñoz, M. C. & Giani, J. F. Modulation of the action of insulin by angiotensin-(1-7). *Clin Sci (Lond)* **126**, 613-630, doi:10.1042/cs20130333 (2014).
- 34 Jiang, F. *et al.* Angiotensin-converting enzyme 2 and angiotensin 1-7: novel therapeutic targets. *Nat Rev Cardiol* **11**, 413-426, doi:10.1038/nrcardio.2014.59 (2014).

- 35 Zhao, L. *et al.* Insulin-degrading enzyme as a downstream target of insulin receptor signaling cascade: implications for Alzheimer's disease intervention. *J Neurosci* **24**, 11120-11126, doi:10.1523/jneurosci.2860-04.2004 (2004).
- 36 Colonna, M. & Butovsky, O. Microglia Function in the Central Nervous System During Health and Neurodegeneration. *Annu Rev Immunol* **35**, 441-468, doi:10.1146/annurev-immunol-051116-052358 (2017).
- 37 Saijo, K. & Glass, C. K. Microglial cell origin and phenotypes in health and disease. *Nat Rev Immunol* **11**, 775-787, doi:10.1038/nri3086 (2011).
- 38 Kelley, N., Jeltama, D., Duan, Y. & He, Y. The NLRP3 Inflammasome: An Overview of Mechanisms of Activation and Regulation. *Int J Mol Sci* **20**, doi:10.3390/ijms20133328 (2019).
- 39 Youm, Y. H. *et al.* The ketone metabolite β -hydroxybutyrate blocks NLRP3 inflammasome-mediated inflammatory disease. *Nat Med* **21**, 263-269, doi:10.1038/nm.3804 (2015).
- 40 Chiarini, A., Gui, L., Viviani, C., Armato, U. & Dal Prà, I. NLRP3 Inflammasome's Activation in Acute and Chronic Brain Diseases-An Update on Pathogenetic Mechanisms and Therapeutic Perspectives with Respect to Other Inflammasomes. *Biomedicines* **11**, doi:10.3390/biomedicines11040999 (2023).
- 41 Dai, Y., Dai, D., Wang, X., Ding, Z. & Mehta, J. L. DPP-4 inhibitors repress NLRP3 inflammasome and interleukin-1 β via GLP-1 receptor in macrophages through protein kinase C pathway. *Cardiovasc Drugs Ther* **28**, 425-432, doi:10.1007/s10557-014-6539-4 (2014).
- 42 Chidambaram, H., Das, R. & Chinnathambi, S. Interaction of Tau with the chemokine receptor, CX3CR1 and its effect on microglial activation, migration and proliferation. *Cell Biosci* **10**, 109, doi:10.1186/s13578-020-00474-4 (2020).
- 43 Pipatpiboon, N., Pratchayasakul, W., Chattipakorn, N. & Chattipakorn, S. C. PPAR γ agonist improves neuronal insulin receptor function in hippocampus and brain mitochondria function in rats with insulin resistance induced by long term high-fat diets. *Endocrinology* **153**, 329-338, doi:10.1210/en.2011-1502 (2012).
- 44 Pipatpiboon, N., Pintana, H., Pratchayasakul, W., Chattipakorn, N. & Chattipakorn, S. C. DPP4-inhibitor improves neuronal insulin receptor function, brain mitochondrial function

- and cognitive function in rats with insulin resistance induced by high-fat diet consumption. *Eur J Neurosci* **37**, 839-849, doi:10.1111/ejn.12088 (2013).
- 45 Furman, B. L. Streptozotocin-Induced Diabetic Models in Mice and Rats. *Curr Protoc Pharmacol* **70**, 5.47.41-45.47.20, doi:10.1002/0471141755.ph0547s70 (2015).
- 46 Skovsø, S. Modeling type 2 diabetes in rats using high fat diet and streptozotocin. *J Diabetes Investig* **5**, 349-358, doi:10.1111/jdi.12235 (2014).
- 47 Swain, S. K., Chandra Dash, U. & Sahoo, A. K. *Hydrolea zeylanica* improves cognitive impairment in high-fat diet fed-streptozotocin-induced diabetic encephalopathy in rats via regulating oxidative stress, neuroinflammation, and neurotransmission in brain. *Heliyon* **8**, e11301, doi:10.1016/j.heliyon.2022.e11301 (2022).
- 48 Ko, C. Y. *et al.* Alleviative Effect of Alpha-Lipoic Acid on Cognitive Impairment in High-Fat Diet and Streptozotocin-Induced Type 2 Diabetic Rats. *Front Aging Neurosci* **13**, 774477, doi:10.3389/fnagi.2021.774477 (2021).
- 49 Wanrooy, B. J. *et al.* Distinct contributions of hyperglycemia and high-fat feeding in metabolic syndrome-induced neuroinflammation. *J Neuroinflammation* **15**, 293, doi:10.1186/s12974-018-1329-8 (2018).
- 50 Yang, H. T. *et al.* Association between the characteristics of metabolic syndrome and Alzheimer's disease. *Metab Brain Dis* **28**, 597-604, doi:10.1007/s11011-013-9406-2 (2013).
- 51 Kumar, V., Kim, S. H. & Bishayee, K. Dysfunctional Glucose Metabolism in Alzheimer's Disease Onset and Potential Pharmacological Interventions. *Int J Mol Sci* **23**, doi:10.3390/ijms23179540 (2022).
- 52 Meidai, L. *et al.* Comparison between an SGLT2 inhibitor and insulin in tumor-to-tissue contrasts in (18)F-FDG PET imaging of diabetic mice. *Sci Rep* **13**, 18329, doi:10.1038/s41598-023-45094-3 (2023).
- 53 Han, X., Ren, H., Nandi, A., Fan, X. & Koehler, R. C. Analysis of glucose metabolism by (18)F-FDG-PET imaging and glucose transporter expression in a mouse model of intracerebral hemorrhage. *Sci Rep* **11**, 10885, doi:10.1038/s41598-021-90216-4 (2021).
- 54 Jensen, N. J., Wodschow, H. Z., Nilsson, M. & Rungby, J. Effects of Ketone Bodies on Brain Metabolism and Function in Neurodegenerative Diseases. *Int J Mol Sci* **21**, doi:10.3390/ijms21228767 (2020).

- 55 Cai, W., Chong, K., Huang, Y., Huang, C. & Yin, L. Empagliflozin improves mitochondrial dysfunction in diabetic cardiomyopathy by modulating ketone body metabolism and oxidative stress. *Redox Biol* **69**, 103010, doi:10.1016/j.redox.2023.103010 (2024).
- 56 Asif, S. *et al.* Hmgcs2-mediated ketogenesis modulates high-fat diet-induced hepatosteatosis. *Mol Metab* **61**, 101494, doi:10.1016/j.molmet.2022.101494 (2022).
- 57 Shippy, D. C. & Ulland, T. K. Microglial Immunometabolism in Alzheimer's Disease. *Front Cell Neurosci* **14**, 563446, doi:10.3389/fncel.2020.563446 (2020).
- 58 Loera-Valencia, R., Eroli, F., Garcia-Ptacek, S. & Maioli, S. Brain Renin-Angiotensin System as Novel and Potential Therapeutic Target for Alzheimer's Disease. *Int J Mol Sci* **22**, doi:10.3390/ijms221810139 (2021).
- 59 Kanugula, A. K., Kaur, J., Batra, J., Ankireddypalli, A. R. & Velagapudi, R. Renin-Angiotensin System: Updated Understanding and Role in Physiological and Pathophysiological States. *Cureus* **15**, e40725, doi:10.7759/cureus.40725 (2023).
- 60 Mori, J. *et al.* ANG II causes insulin resistance and induces cardiac metabolic switch and inefficiency: a critical role of PDK4. *Am J Physiol Heart Circ Physiol* **304**, H1103-1113, doi:10.1152/ajpheart.00636.2012 (2013).
- 61 Abiodun, O. A. & Ola, M. S. Role of brain renin angiotensin system in neurodegeneration: An update. *Saudi J Biol Sci* **27**, 905-912, doi:10.1016/j.sjbs.2020.01.026 (2020).
- 62 Furiya, Y. *et al.* Renin-angiotensin system blockers affect cognitive decline and serum adipocytokines in Alzheimer's disease. *Alzheimers Dement* **9**, 512-518, doi:10.1016/j.jalz.2012.06.007 (2013).
- 63 Ribeiro, V. T., de Souza, L. C. & Simões, E. S. A. C. Renin-Angiotensin System and Alzheimer's Disease Pathophysiology: From the Potential Interactions to Therapeutic Perspectives. *Protein Pept Lett* **27**, 484-511, doi:10.2174/0929866527666191230103739 (2020).
- 64 Kunvariya, A. D., Dave, S. A., Modi, Z. J., Patel, P. K. & Sagar, S. R. Exploration of multifaceted molecular mechanism of angiotensin-converting enzyme 2 (ACE2) in pathogenesis of various diseases. *Heliyon* **9**, e15644, doi:10.1016/j.heliyon.2023.e15644 (2023).
- 65 Shin, S. J. *et al.* Effect of Sodium-Glucose Co-Transporter 2 Inhibitor, Dapagliflozin, on Renal Renin-Angiotensin System in an Animal Model of Type 2 Diabetes. *PLoS One* **11**,

- e0165703, doi:10.1371/journal.pone.0165703 (2016).
- 66 Chen, Y. & Peng, D. New insights into the molecular mechanisms of SGLT2 inhibitors on ventricular remodeling. *Int Immunopharmacol* **118**, 110072, doi:10.1016/j.intimp.2023.110072 (2023).
- 67 Puglisi, S. *et al.* Effects of SGLT2 Inhibitors and GLP-1 Receptor Agonists on Renin-Angiotensin-Aldosterone System. *Front Endocrinol (Lausanne)* **12**, 738848, doi:10.3389/fendo.2021.738848 (2021).
- 68 Leissring, M. A., González-Casimiro, C. M., Merino, B., Suire, C. N. & Perdomo, G. Targeting Insulin-Degrading Enzyme in Insulin Clearance. *Int J Mol Sci* **22**, doi:10.3390/ijms22052235 (2021).
- 69 Malito, E., Hulse, R. E. & Tang, W. J. Amyloid beta-degrading cryptidases: insulin degrading enzyme, presequence peptidase, and neprilysin. *Cell Mol Life Sci* **65**, 2574-2585, doi:10.1007/s00018-008-8112-4 (2008).
- 70 Gejl, M. *et al.* In Alzheimer's Disease, 6-Month Treatment with GLP-1 Analog Prevents Decline of Brain Glucose Metabolism: Randomized, Placebo-Controlled, Double-Blind Clinical Trial. *Front Aging Neurosci* **8**, 108, doi:10.3389/fnagi.2016.00108 (2016).
- 71 Gilbert, M. P. & Pratley, R. E. GLP-1 Analogs and DPP-4 Inhibitors in Type 2 Diabetes Therapy: Review of Head-to-Head Clinical Trials. *Front Endocrinol (Lausanne)* **11**, 178, doi:10.3389/fendo.2020.00178 (2020).
- 72 Wu, C. Y. *et al.* Relationships between memory decline and the use of metformin or DPP4 inhibitors in people with type 2 diabetes with normal cognition or Alzheimer's disease, and the role APOE carrier status. *Alzheimers Dement* **16**, 1663-1673, doi:10.1002/alz.12161 (2020).
- 73 Birajdar, S. V., Mazahir, F., Alam, M. I., Kumar, A. & Yadav, A. K. Repurposing and clinical attributes of antidiabetic drugs for the treatment of neurodegenerative disorders. *Eur J Pharmacol* **961**, 176117, doi:10.1016/j.ejphar.2023.176117 (2023).
- 74 Yuan, Y. *et al.* Effects of DPP4 Inhibitors as Neuroprotective Drug on Cognitive Impairment in Patients with Type 2 Diabetes Mellitus: A Meta-Analysis and Systematic Review. *Int J Endocrinol* **2024**, 9294113, doi:10.1155/2024/9294113 (2024).
- 75 Lindborg, J. A. *et al.* Molecular and cellular identification of the immune response in peripheral ganglia following nerve injury. *J Neuroinflammation* **15**, 192,

- doi:10.1186/s12974-018-1222-5 (2018).
- 76 Liu, S. Q., Xie, Y., Gao, X., Wang, Q. & Zhu, W. Y. Inflammatory response and MAPK and NF- κ B pathway activation induced by natural street rabies virus infection in the brain tissues of dogs and humans. *Virology* **17**, 157, doi:10.1186/s12985-020-01429-4 (2020).
- 77 Kino, T., Khan, M. & Mohsin, S. The Regulatory Role of T Cell Responses in Cardiac Remodeling Following Myocardial Infarction. *Int J Mol Sci* **21**, doi:10.3390/ijms21145013 (2020).
- 78 Guerra-Espinosa, C., Jiménez-Fernández, M., Sánchez-Madrid, F. & Serrador, J. M. ICAMs in Immunity, Intercellular Adhesion and Communication. *Cells* **13**, doi:10.3390/cells13040339 (2024).
- 79 Zeng, J. *et al.* The mechanism of microglia-mediated immune inflammation in ischemic stroke and the role of natural botanical components in regulating microglia: A review. *Front Immunol* **13**, 1047550, doi:10.3389/fimmu.2022.1047550 (2022).
- 80 Ferro, A., Auguste, Y. S. S. & Cheadle, L. Microglia, Cytokines, and Neural Activity: Unexpected Interactions in Brain Development and Function. *Front Immunol* **12**, 703527, doi:10.3389/fimmu.2021.703527 (2021).
- 81 Gaire, B. P. Microglia as the Critical Regulators of Neuroprotection and Functional Recovery in Cerebral Ischemia. *Cell Mol Neurobiol* **42**, 2505-2525, doi:10.1007/s10571-021-01145-9 (2022).
- 82 Gao, C., Jiang, J., Tan, Y. & Chen, S. Microglia in neurodegenerative diseases: mechanism and potential therapeutic targets. *Signal Transduct Target Ther* **8**, 359, doi:10.1038/s41392-023-01588-0 (2023).
- 83 Jayashankar, S. S., Tajul Arifin, K. & Nasaruddin, M. L. β -Hydroxybutyrate Regulates Activated Microglia to Alleviate Neurodegenerative Processes in Neurological Diseases: A Scoping Review. *Nutrients* **15**, doi:10.3390/nu15030524 (2023).
- 84 Bolós, M. *et al.* Absence of CX3CR1 impairs the internalization of Tau by microglia. *Mol Neurodegener* **12**, 59, doi:10.1186/s13024-017-0200-1 (2017).
- 85 Pawelec, P., Ziemka-Nalecz, M., Sypecka, J. & Zalewska, T. The Impact of the CX3CL1/CX3CR1 Axis in Neurological Disorders. *Cells* **9**, doi:10.3390/cells9102277 (2020).
- 86 Kim, H. J., Kim, H., Lee, J. H. & Hwangbo, C. Toll-like receptor 4 (TLR4): new insight

immune and aging. *Immun Ageing* **20**, 67, doi:10.1186/s12979-023-00383-3 (2023).

APPENDICES

AD, Alzheimer's disease; T2D, type 2 diabetes mellitus; SGLT2-i, sodium–glucose cotransporter-2 inhibitor; DPP4-i, dipeptidyl peptidase-4 inhibitor; HFD, high-fat diet; PO, orally; pTau, hyperphosphorylated tau; A β , amyloid β ; NLRP3, NLR family pyrin domain containing 3; APP, amyloid precursor protein; GSK3 β , glycogen synthase kinase-3 β ; NFTs, neurofibrillary tangles; fAD, familial AD; PSEN1, presenilin-1; PSEN2, presenilin-2; sAD, sporadic AD; IRS, insulin receptor substrates; IRS1, insulin receptor substrates 1; IRS2, insulin receptor substrates 2; PI3K, phosphoinositide 3-kinase; Akt, protein kinase B; PKC ζ , protein kinase C ζ ; PKC λ , protein kinase C λ ; mTOR, mammalian target of rapamycin; IKK, inhibitor of nuclear factor- κ B kinase; CD14, cluster of differentiation 14; CD36, cluster of differentiation 36; CD47, cluster of differentiation 47; TLR, toll-like receptor; TLR4, toll-like receptor 4; GLP-1, glucagon-like peptide-1; GLP-1R, glucagon-like peptide-1 receptor; GIP, glucose-dependent insulinotropic polypeptide; ND, normal chow diet; STZ, streptozotocin; IP, intraperitoneally; BG, blood glucose level; BW, body weight; ITT, insulin tolerance test; GTT, glucose tolerance test; HOMA-IR, homeostatic model assessment for insulin resistance; NORT, novel object recognition test; MWM, morris water maze; ¹⁸F-FDG, ¹⁸F-fluorodeoxyglucose; ¹⁸F-FDG-PET, ¹⁸F-FDG-positron-emission tomography; WB, western blotting; IHC, immunohistochemistry; CTX, cortex; HIPPO, hippocampus; PFA, paraformaldehyde; PBS, phosphate-buffered saline; BSA, bovine serum albumin; TBS, tris-buffered saline; TBS-T, tris-buffered saline containing tween 20; HRP, horseradish peroxidase; DAPI, 6-diamidino-2-phenylindole; pIRS1, phospho-IRS1; pAkt, phospho-Akt; pGSK3 β , phospho-GSK3 β ; GLUT1, glucose transporter 1; GLUT3, glucose transporter 3; GLUT4, glucose transporter 4; MAP2, microtubule-associated protein 2; ACE2, angiotensin converting enzyme-2; Ang (1-7)/MasR, angiotensin (1-7)/mitochondrial assembly receptor; IDE, insulin-degrading enzyme; TMEM119, transmembrane protein 119; IL-4, interleukin 4; IL-1 β , interleukin 1 β ; CD206, mannose receptor; CD86, cluster of differentiation 86; LC3, microtubule-associated protein 1A/1B-light chain 3; CX3CR1, C-X3-C motif chemokine receptor 1; NF- κ B, nuclear factor κ -light-chain-enhancer of activated B cells; qPCR, quantitative polymerase chain reaction; ANOVA, one-way analysis of variance analysis; S.E.M, standard error of the mean; GLUTs, glucose transporters; AcAc, acetoacetate; BHB, β -hydroxybutyrate; HMGCL, 3-hydroxy-3-methylglutaryl-CoA lyase;

HMGCS2, 3-hydroxy-3-methylglutaryl-CoA synthase 2; BDH1, 3-hydroxybutyrate dehydrogenase 1; PPAR- α , peroxisome proliferator-activated receptor α ; MCT1, monocarboxylate transporter 1; MCT2, monocarboxylate transporter 2; SMCT1, sodium-coupled monocarboxylate transporter 1; SMCT2, sodium-coupled monocarboxylate transporter 2; Q1, quadrant 1; Q4 quadrant 4; RAS, renin-angiotensin system; Ang I, angiotensin I; Ang II, angiotensin II; ACE1, angiotensin converting enzyme-1; AT1R, Ang II receptor type 1; M1, pro-inflammatory phenotype; M2, anti-inflammatory phenotype; CD54, cluster of differentiation 54; IFN- γ , interferon γ ; IL-16, interleukin 16; M-CSF, colony stimulating factor 1; CXCL12, C-X-C motif chemokine 12; TIMP-1, tissue inhibitor matrix metalloproteinase 1; IL-18, interleukin 18; FFA, free fatty acids; HMG-CoA, 3-hydroxy-3-methylglutaryl-CoA; β -OHB, β -hydroxybutyrate; TCA, tricarboxylic acid; Cox2, cyclooxygenase-2; iNOS, inducible nitric oxide synthase; IL-6, interleukin 6; TNF, tumor necrosis factor; CNS, central nervous system; cAMP, cyclic adenosine monophosphate; PKA, protein kinase A; CD4, cluster of differentiation 4; ROS, reactive oxygen species; ASC, caspase recruitment domain; CX3CL1, C-X3-C motif ligand 1; TREM2, triggering receptor expressed on myeloid cells 2; PAMPs, pathogen-associated molecular patterns; DAMPs, damage-associated molecular patterns; MyD88, myeloid differentiation primary response 88

ABSTRACT IN KOREAN

전신 대사 조절을 통한 알츠하이머병 유사 병리 및 인지기능 장애 완화 기전

알츠하이머병 (AD)과 제2형 당뇨병 (T2D)은 인슐린 저항성을 포함한 공통적인 특징을 공유한다. 뇌의 인슐린 저항성은 AD 발병의 주요 요인으로 알려져 있으며 최근 연구를 통해 항 당뇨병 약물인 나트륨-포도당 공동수송체-2 억제제 (SGLT2-i)와 디펩티딜 펩티다제-4 억제제 (DPP4-i)가 인슐린 감수성을 개선하고 신경 보호 기능을 제공하는 것이 알려졌다. 하지만 이 두 가지 억제제가 뇌 대사에 미치는 정확한 메커니즘은 아직 명확하게 밝혀지지 않았다.

본 연구에서는 고지방 식이 및 단일 용량의 스트렙토조토신을 이용하여 T2D-AD 마우스 모델을 구현하였고, 이후 7주동안 SGLT2-i와 DPP4-i를 투여하였다. SGLT2-i 및 DPP4-i는 T2D-AD 마우스 모델에서 혈당과 체중을 감소시키고, 말초와 뇌 내 인슐린 감수성을 효과적으로 개선하여 해마 의존적 학습과 기억 능력 및 인지 기능을 크게 향상시켰다. 흥미롭게도 SGLT2-i와 DPP4-i는 각각 과인산화된 타우 (pTau) 수준과 아밀로이드 β ($A\beta$) 축적 감소에 크게 영향을 미쳤다. SGLT2-i는 안지오텐신 전환 효소-2/안지오텐신 (1-7)/미토콘드리아 조립 수용체 축을 통해 pTau 축적을 감소시킨 반면, DPP4-i는 인슐린 분해 효소 수준을 증가시켜 $A\beta$ 축적을 감소시켰다. 또한 SGLT2-i와 DPP4-i를 통한 포도당 및 케톤 대사의 변화는 미세아교세포의 NLRP 인플라마솜 조절을 억제하여 미세아교세포의 활성화를 변화시켰다. SGLT2-i와 DPP4-i는 각각 G-단백질 결합 수용체 13과 툴유사수용체4를 통해 NLRP3 인플라마솜에 관여하였고, 표현형을 변화시켜 pTau 및 $A\beta$ 축적으로 인한 신경 염증 반응을 개선하였다.

이러한 결과들은 SGLT2-i와 DPP4-i가 뇌의 인슐린 신호전달 및 염증 반응에 관여하여 신경 퇴행을 조절하고, 서로 다른 메커니즘을 통해 T2D-AD 마우스 모델에서 AD 유사 병리 및 인지 기능 장애를 예방하는 의미 있는 연구라고 할 수 있다.

핵심 되는 말 : 알츠하이머, 제2형 당뇨, SGLT2 억제제, DPP4 억제제, 인슐린 신호 전달, 신경염증